Word count
Total word count: 3554
Abstract: 142
Number of references: 95
Number of figures: 6

The gut microbiome and colonic pH shape the peripheral immune landscape in humans

Short title: Gut microbiome, pH and immune system

Evany Dinakis[1,2], Dakota Rhys-Jones[3], Leticia Camargo Tavares[1,2], Chaoran Yang[1,2], CK Yao[3], Daniel So[3], Dovile Anderson[4], Darren Creek[5], Stephen J. Turner[6], Peter R. Gibson[3], Charles R. Mackay[7,8], Joanne A. O'Donnell[1,2], Jane Muir[3], Francine Z. Marques[1,2,9*]

[1]Hypertension Research Laboratory, Department of Pharmacology, Biomedical Discovery Institute, Faculty of Medicine, Nursing and Health Sciences, Monash University, Clayton VIC 3800, Australia; [2]Victorian Heart Hospital, Monash University, Clayton VIC, 3168, Australia; [3]Department of Gastroenterology, Central Clinical School, Monash University, Melbourne, 3000, Victoria, Australia; [4]Monash Proteomics and Metabolomics Facility, Monash Institute of Pharmaceutical Sciences, Monash University, Parkville, VIC 3052, Australia; [5]Monash Biomedical Imaging, Monash University, Clayton, VIC 3168, Australia; [6]Department of Microbiology, Immunity Theme, Biomedical Discovery Institute, Monash University, Clayton, VIC, Australia; [7]Department of Microbiology, Biomedicine Discovery Institute, Monash University, Clayton, VIC 3800, Australia; [8]School of Pharmaceutical Sciences, Shandong Analysis and Test Center, Qilu University of Technology (Shandong Academy of Sciences), Jinan, 250014, China; [9]Baker Heart and Diabetes Institute, Melbourne, VIC 3000, Australia.

***Corresponding author**: Prof Francine Marques, Hypertension Research Laboratory, Victorian Heart Institute, Level 2, Victorian Heart Hospital, 631 Blackburn Road, Clayton, VIC 3168, Monash University, Melbourne, Australia, Phone: +61-03-9905 6958. E-mail: francine.marques@monash.edu

Abstract

The physicochemical environment of the gut, particularly colonic pH, plays a critical role in shaping host-microbe interactions; yet its influence on systemic immunity in humans remains poorly understood. Here, we integrated faecal metagenomics, plasma short-chain fatty acid (SCFA) profiling, SmartPill wireless pH-motility capsule data, and deep immunophenotyping of peripheral blood mononuclear cells in 54 participants to investigate the relationship between colonic pH, microbial metabolism, and immune tone. We found that lower colonic pH was associated with cytokine-producing CD8+ T cells, while higher pH correlated with pre-exhausted CD8+ T cells and elevated neutrophil populations. Metagenomic analyses revealed species-level associations within the genus *Eubacterium*, linked to colonic pH and peripheral immune profiles. These findings suggest that microbial metabolic activity and gut pH jointly modulate immune tone beyond the gut in humans, establishing a functional axis between microbial fermentation, physicochemical gut conditions, and systemic immunity.

Introduction

The gastrointestinal (GI) tract orchestrates tightly regulated physiological gradients, among which pH plays a central role in shaping microbial and immune dynamics[1]. pH dynamics across the GI tract are markedly heterogenous[1,2]. The large intestine presents a mildly acidic to neutral pH (5.5–7), with the proximal colon maintaining a more acidic environment (pH ~5.5-6.0), whereas the distal colonic luminal pH is typically more alkaline (~6.5-7.0)[3,4]. This spatial variation parallels the distribution of the gut microbiome[5-7]. Microbial density is low in the upper GI tract but peaks in the colon, which harbours the most diverse and metabolically active communities, thus serving as a key site for host-microbiome interactions[8,9].

Colonic pH is shaped by microbial metabolic activity[10,11], while pH itself influences the composition and activity of the gut microbiome[12,13]. This bidirectional interaction, therefore, tightly links microbial function with the physiochemical environment of the colon. Diet is a key modulator of this interaction; diets rich in complex carbohydrates such as fibre, for example, enhance microbial diversity and fermentation, leading to the production of short-chain fatty acids (SCFAs)[14,15]. These acidic metabolites lower colonic luminal and interstitial fluid pH[16], making colonic pH a dynamic parameter responsive to both microbial and dietary inputs.

The GI tract is also a major immunological organ[17], with extensive crosstalk between resident microbes and host immunity. Studies using germ-free animal models revealed that the gut microbiome is essential for the maturation of both intestinal and systemic immunity[18,19], leading to impaired lymphoid tissue development and T cell function, and reduced immunoglobulin production[20-22]. Yet, most mechanistic insights have largely centred on mucosal immunity[23] and experimental models. The extent to which the gut microbiome shapes the peripheral immune system in humans remains poorly understood.

Here, we present an integrated systems-level analysis of host microbiome–intestinal pH–immune interactions in a human cohort. By combining faecal shotgun metagenomic sequencing, *in vivo* colonic intraluminal pH profiling using the SmartPill wireless pH-motility capsule, and deep immunophenotyping of peripheral blood mononuclear cells (PBMCs), we show that colonic pH has an important immunomodulatory effect on the peripheral immune system. Specifically, we implicate *Eubacterium* species and their metabolic input in amino acid and nucleotide metabolism and biosynthesis pathways as key drivers of peripheral

immunomodulation, suggesting colonic pH may be a functional mediator of microbiome-systemic immune crosstalk.

Results

Mapping colonic pH gradients using a wireless pH-motility capsule (SmartPill)

Fifty-four healthy participants completed the trial, of whom 41% were female. Participants had a mean age of 49 ± 12.9 years and body mass index (BMI) of 27.0 ± 3.7 kg m^{-2} (Figure 1, Table S1). The SmartPill software provides median, minimum, and maximum pH values – these provide proxy values for different intestinal sites. The minimum colonic value indicates the ascending colon, while the maximum colonic pH indicates distal colonic and sigmoid/rectum pH (Figure 2A-B). To map the heterogeneity of luminal pH across different colonic regions, we divided the colon into four equal quartiles, as previously reported[10]. This was performed based on transit time by dividing the total time in the colon into four equal quartiles, with the assumption that transit time would have been the same across all segments of the colon. These quartiles are thought to approximately correspond to the main regions of the large intestine (Figure 2A). Indeed, our data fitted with the expected pattern of pH distribution along the colon (Figure 2B), whereby colonic minimum pH was significantly correlated with first and second quartile intraluminal pH (Figures 2C-D), colonic median pH was significantly correlated with first to third quartiles (Figures 2E-G), and colonic maximum pH was correlated with second to fourth quartiles (Figures 2H-J).

Colonic pH correlates with peripheral immune cells and SCFAs

Gut transit time is an important physiological variable that integrates nutrient absorption and microbial fermentation[24], thus its link with intraluminal pH represents an interesting avenue for investigation. Longer whole-gut (WGTT), small and large bowel (SLBTT) and colonic transit time (CTT) were associated with higher (more basic) pH in quartiles two through four, but not quartile one (Figure 2K). Strikingly, higher daily dietary fibre intake was associated with lower, or more acidic, minimum and quartile one colonic pH (Figure 2K). The main by-product of fermentable fibre produced by the gut microbiome inhabiting the large intestine is SCFAs[25], acidic immunomodulatory metabolites that can profoundly influence physiological outcomes such as colonic pH[16]. Only higher plasma propionic acid levels were associated with lower quartile one, two and four colonic pH (Figure 2K).

We further analysed potential relationships between colonic pH and 121 peripheral immune cell populations and sub-types, including activation and cytokine expression across these cell

types. We identified varying associations with 14 different peripheral immune cell subsets across all seven colonic pH variables (Figure 2K). Overall, these suggest that colonic pH is associated with peripheral immunomodulation. Notably, 10 associations were with the T cell lineage; for example, elevated numbers of CD8+ central memory T cells and a dual cytokine-producing (interferon-γ [IFNγ]/ tumour necrosis factor-α [TNFα]) population of activated CD8+ T cells were associated with lower colonic minimum pH. Conversely, programmed cell death protein-1 (PD-1)+ CD8+, activated PD-1+ CD8+ T cells, IFNγ-producing natural killer (NK) cells and neutrophils were associated with more basic colonic pH.

Correlation analyses between plasma SCFA levels and the peripheral immune system further revealed 17 significant associations, of which 14 were negatively associated with isovaleric acid and were comprised almost entirely of CD4+ T cell subsets (Figure 2L). Plasma butanoic acid was positively associated with B cells and PD-1+ CD8+ T cells, whilst lower plasma acetic and butanoic acid were associated with the production of both interleukin (IL)-2 and TNFα by CD161+ CD4+ T cells (Figure 2L).

A distinct subset of pre-exhausted CD8+ T cells consistently underpins gut microbiome and colonic pH associations

Upon persistent antigen stimulation, such as during chronic infection or cancer, activated T cells can enter a state of functional decline known as exhaustion[26,27]. This transition is marked by sustained expression of inhibitory receptors, including PD-1 and TIM-3, and diminished proliferative capacity, often linked to impaired IL-2 signalling and reduced cytokine production (i.e., TNFα and IFNγ)[28-30] (Figure S1A). For example, in melanoma patients, TIM-3+ PD-1+ tumour-specific CD8+T cells were more dysfunctional than TIM-3- PD-1+ and TIM-3- PD-1- T cells, producing less IFN-γ, TNF-α and IL-2[29]. However, T cells can enter a transitional pre-exhausted state, typically marked by reduced IL-2 production and consequently diminished proliferative capacity[31]. This state is characterized by elevated PD-1 expression in the absence of other inhibitory receptors such as TIM-3[32], while retaining functional competence and the ability to produce effector cytokines[33,34] (Figure S1A). We performed a sensitivity analysis focusing on the functionality of PD-1+ CD8+ T cells and found that these cells retained a pre-exhausted phenotype, as evidenced by a lack of TIM-3 and IL-2 expression (Figure S1B). Moreover, taxonomic profiling identified 14 differentially abundant taxa specifically positively associated with these pre-exhausted CD8+ T cells (Figure S1C).

Distal colonic pH is associated with the gut microbiome and associated metabolic pathways

To assess differences in the gut microbiome in relation to colonic pH measurements, we calculated α- and β-diversity metrics from shotgun metagenome data. We found no association between α-diversity and colonic pH (Table S2). However, β-diversity analyses revealed distinct gut microbiome differences across colonic pH in quartile one (Table S2). Specifically, based on unweighted UniFrac distances, quartile one colonic pH explained 3.5% of the observed variation in the gut microbiome composition (P=0.014, Table S2), suggesting compositional differences characterised by the presence/absence of unique microbial taxa.

Taxonomic profiling analysis revealed that one bacterial species, *Blautia schinkii*, was associated with colonic pH in quartile four (q=0.0143; Figure S2). Functional profiling analysis revealed 169 positive associations between differentially abundant species-specific metabolic pathways and quartile four (Figure 3A). Eighty metabolic pathways, categorised by biological function, were stratified across eight bacterial species (Table S3, Figure 3A). Notably, we did not identify any significant *Blautia schinkii*-specific metabolic pathways associations with quartile four colonic pH. Our analysis instead showed that *Bifidobacterium pseudocatenulatum*, a species that thrives on complex carbohydrate fermentation[35], exhibited the strongest associations across all seven classifications of metabolic pathways, particularly with pathways involved in amino acid biosynthesis.

Gut microbiome species and metabolic pathways are associated with the peripheral immune system

Next, we sought to identify specific taxa and microbial pathways associated with the peripheral immune system. Sixty two taxa, grouped at the genus level, were associated with 64 immune cell populations/sub-types, stratified by immune subset categories, resulting in 380 associations in total (Figure 3B, Tables S4 and S5). Although associations were present across all immune groups, associations stemming from the CD4+ and CD8+ T cell categories prevailed. Notably, these clusters were predominantly composed of single and double pro-inflammatory cytokine-producing early and late-activated populations (CD69+ and human leukocyte antigen-DR isotype [HLA-DR]+, respectively), as well as PD-1+ expressing cells amongst others (Table S4). We also identified that differentially abundant taxa classified as 'Other' exhibited the strongest associations with both CD4+ and CD8+ T cell clusters, followed by the genus *Merdicola*, comprising two unique, genetically similar bacterial taxa *Merdicola sp001915925*

and *Merdicola sp900555085* (Table S5). Taxa grouped into the 'Other' category also predominated in associations with the peripheral immune system overall, comprising taxa yet to be characterised (Table S4). At the functional level, 945 species-specific metabolic pathway associations were identified with the peripheral immune system, linked by eight bacterial species (Figure 3C). Thirty-five metabolic pathways, categorised based on biological function, were associated with 60 peripheral immune cell populations/sub-types (Tables S3 and S4). Consistently, CD4+ and CD8+ T cell clusters showed the largest and strongest associations, again predominated by subsets including single (i.e., IFNγ, IL-17A and TNFα) and double (i.e., IFNγ/TNFα IL-2/TNFα) pro-inflammatory cytokine-producing activated cell types (Figure 3C & Table S4). Moreover, pathways involved in nucleotide metabolism and biosynthesis had the most pronounced associations across the peripheral immune system (Figure 3C, Table S3 and Table S4). Among the species identified as differentially abundant in the taxonomic profiling analysis, four remained consistent, linking the peripheral immune system and bacterial metabolic output: *Clostridium sp AM22 11AC*, *Eubacterium ventriosum*, *Holdemanella biformis* and *Streptococcus thermophilus*. We identified that *Holdemanella biformis* exhibited the highest functional metabolic contribution across all pathway groups (excluding lipid and membrane metabolism) and accounted for the greatest number of associations with the peripheral immune system (Figure 3C).

Holdemanella biformis **and its metabolic pathways are associated with the peripheral immune system**

To delineate this further, we explored the relationship between *Holdemanella biformis,* formally *Eubacterium biforme*[36], and the peripheral immune system more closely, revealing positive associations with 11 peripheral immune cell types (Figure 4A). More than 50% of associated immune cells were T cell subsets, specifically IL-17A-producing and PD-1+ CD4+ and CD8+ T cells. Strikingly, we identified two natural killer (NK) cell populations producing TNFα, a well-characterised pro-inflammatory cytokine that reportedly governs whether *Holdemanella biformis* drives inflammation or resolution[37]. Moreover, we demonstrated that the functional metabolic activity of *Holdemanella biformis* spans 37 pathways and exhibited varying positive associations with 21 peripheral immune cell populations and sub-types, 11 of which correspond to the immune subsets identified via taxonomic profiling (Figure 4B). Among these, four pathways consistently prevailed with the strongest associations across the suite of immune cell subsets; the methylerythritol phosphate pathway I, superpathway of L-tyrosine biosynthesis and superpathway of thiamine diphosphate biosynthesis III, as well as

the flavin biosynthesis I pathway being associated with 18 and 19 subsets, respectively (Figure 4B).

Eubacterium species and associated metabolic pathways link colonic pH in quartile four and the peripheral immune system

To investigate the interplay between colonic pH, gut microbiome, and the peripheral immune system, we performed an integrated analysis combining taxonomic and functional profiling. This revealed a genus-level convergence centred on *Eubacterium*, with distinct species showing differential associations across biological domains (Figure 5). *Eubacterium ventriosum* was consistently linked to peripheral immune cell profiles, suggesting a mechanistic role in systemic immune modulation. In contrast, *Eubacterium rectale* and *Eubacterium sp CAG 38* were associated with colonic pH in quartile four. Specifically, taxonomic differential abundance analysis showed that three immune cell types, C-C chemokine receptor type 7 (CCR7)+, central memory (CM) CD8+ T cells, and non-classical monocytes, were positively associated with *Eubacterium ventriosum* (Figure 5A). These remained prominent amongst 13 other peripheral immune cell types positively associated with metabolic pathways of *Eubacterium ventriosum* (Figure 5B). Notably, non-classical monocytes exhibited the strongest and largest associations with 15 of the 16 metabolic pathways, whilst the purine ribonucleoside degradation pathway had the highest number of associations across the suite of immune cell subsets, predominated by pro-inflammatory T cell subsets including IL-17A-producing and PD-1 expressing CD4+ and CD8+ T cells, as well as TNFα-producing NK and T cell populations (Figure 5B).

Whilst we did not identify any *Eubacterium ventriosum*-specific metabolic pathway associated with colonic pH, we profiled another two metabolically active *Eubacterium* species (Figure 5C). *Eubacterium rectale* facilitated the positive association between colonic pH in quartile four with the D-galactose degradation, or Leloir, pathway. In contrast, *Eubacterium sp CAG 38*-specific pathways, including those involved in amino acid and nucleotide biosynthesis, accounted for the remaining positive associations with quartile four (Figure 5C).

To better elucidate the biological relevance of these findings, we examined overlapping pathways across both functional analyses and found that the metabolic activity of *Eubacterium sp CAG 38* and *Eubacterium ventriosum* involved in the L-valine (amino acid) biosynthesis pathway and the purine ribonucleoside degradation and UMP biosynthesis II and III pathways, classed as nucleotide metabolism and biosynthesis pathways respectively, linked colonic pH

in the fourth quartile and the peripheral immune system (Figure 6). Twelve cell types prevailed, reinforcing a more pro-inflammatory profile characterised by IL-17A-producing CD4+ T cells, non-classical monocytes and TNFα-producing NK and T cell subsets, all of which have been consistently reported throughout. Additionally, PD-1-expressing T cells, particularly CD8+ T cells, repeatedly emerged as a recurrent feature.

Discussion

While the gut microbiome is known to influence mucosal immunity, its impact on systemic immune tone via physicochemical cues such as colonic pH remains poorly defined in humans. Here, we demonstrated that both colonic luminal and regional pH are associated with peripheral immunomodulation. Specifically, lower colonic luminal pH was associated with the enrichment of T cell populations, particularly CD8+ T cells, including cytokine-producing and pre-exhausted phenotypes. A more acidic colonic pH, primarily driven by SCFA production from fibre fermentation[16], may foster a metabolically active gut environment that supports functional CD8+ T cell responses. These cells, traditionally recognised for their role in antiviral and cytotoxic responses[38,39], are highly responsive to environmental cues such as microbial-derived metabolites and inflammatory cytokines[40-42]. These environmental cues can potentiate CD8+ T cell effector responses and enhance the secretion of key pro-inflammatory mediators including IFNγ and TNFα[43-45]. In contrast, a more alkaline pH, typically associated with depletion of fibre substrates for fermentation and reduced SCFA levels[16], may favour PD-1+ exhausted-like CD8+ phenotypes, linked to chronic diseases such as cancer[27,46] and high blood pressure[47]. Additionally, higher neutrophil counts were associated with a more alkaline colonic pH[48], commonly observed in metabolic syndrome[49]. Together, these findings suggest that colonic pH, shaped by the gut microbiome and microbial fermentation, may serve as a functional cue for peripheral immune activation, linking gut metabolic tone to systemic immune outcomes.

A key finding was *Eubacterium* species mediating the relationship between colonic pH and peripheral immune responses in humans. This genus, a core component of the human gut microbiome, exhibits widespread colonisation across diverse populations spanning Africa[50], Australia[51], Europe[52], Asia[53] and the Americas[54,55]. Our analyses revealed that, while functionally distinct, *Eubacterium sp CAG 38* and *Eubacterium ventriosum* metabolically converge in the L-valine biosynthesis pathway, providing a mechanistic link between colonic pH (i.e., quartile 4) and 11 peripheral immune cells, 7 of which are T cell subtypes. Valine, an

essential branched-chain amino acid, serves as a fundamental protein building block and an immunomodulatory metabolite[56]. L-valine enhances PI3K/Akt1 signalling in macrophages[57], key antigen-presenting cells of the innate immune system[58]. Pharmacological inhibition of PI3K partially attenuates L-valine-induced bacterial phagocytosis[57], aligning with prior evidence that PI3K/Akt signalling governs macrophage phagocytic function[59,60]. Notably, we observed a strong association with non-classical monocytes, precursors of macrophages, which also present antigen-processing capabilities under inflammatory conditions[61]. Moreover, altered valine tRNA biogenesis augments mitochondrial energy production in T cell acute lymphoblastic leukemia[62], underscoring valine's broader role in supporting immune cell bioenergetics across both innate and adaptive compartments. These findings position *Eubacterium*-derived valine metabolism as a mechanistic bridge between gut physicochemical gradients and systemic immune tone.

In parallel, both species showed strong associations with the purine ribonucleoside degradation pathway. Uric acid, the end product of purine metabolism[63], can accumulate in response to diets high in purine-rich foods (i.e., red meat, seafood) or low in fibre, shifting microbial activity toward increased uric acid production[64]. As a recognised damage-associated molecular pattern[65,66], uric acid activates antigen-presenting cells – including monocytes/macrophages and dendritic cells – prompting the upregulation of co-stimulatory molecules such as CD80 and CD86[67]. This enhanced expression facilitates the activation of CD8+ T cells, driving their proliferation and effector function[68,69]. Conversely, pharmacological inhibition of uric acid production suppresses CD8+ T cell activation and effector function, as evidenced by reduced CD69 and IFN-γ expression, respectively, and proliferative capacity due to diminished secretion of IL-2[70]. These findings suggest that sustained upregulation of *Eubacterium ventriosum*-mediated purine catabolism may elevate uric acid levels, contributing to the altered CD8+ T cell landscape we observed, such as loss of IL-2 production in the PD-1+ CD8+ T cells consistent with a pre-exhausted phenotype.

Under physiological conditions, PD-1 is transiently induced upon T cell activation to limit excessive T-cell receptor signalling and maintain immune homeostasis[71]. Under conditions of chronic infection and cancer, however, persistent antigen exposure drives sustained PD-1 expression on CD8+ T cells, contributing to their progressive functional exhaustion[26,27,72]. In cancer, exhausted T cells accumulate within the tumour microenvironment, and are a key target of immune checkpoint blockade[46]. For example, therapeutic inhibition of PD-1 and its ligand PD-L1, otherwise known as the PD-1/PD-L1 axis[73], has shown clinical efficacy in numerous

types of cancer and acts primarily by reinvigorating effector function and restoring anti-tumour immunity[74,75]. Importantly, butyrate-producing bacteria, such as those from the *Eubacterium* genus[85,86], including *Eubacterium R sp003526845*, which we identified as differentially abundant, can modulate the epigenetic and metabolic programming of CD8+ T cells, thereby influencing the expression of exhaustion markers such as PD-1[76]. Through enhanced histone acetylation and improved mitochondrial function, butyrate supports effector activity and mitigates terminal exhaustion, ultimately enhancing responsiveness to PD-1 checkpoint blockade[77-79]. This mechanistic link may underlie the positive correlation we observed between PD-1+ CD8+ T cells and plasma butanoic acid levels. It may explain why these profiled PD-1+ CD8+ T cells remain functional (i.e., IFNγ-producing) and are not terminally exhausted. Butyrate also plays a potent role in regulating neutrophil activity by suppressing inflammation through pathways such as GPR43 signalling[80,81]. Consequently, reduced SCFA levels, often indicated by a more alkaline colonic pH, may contribute to the elevated neutrophil counts observed.

Another key finding concerned *Holdemanella*, which has been associated with improved outcomes in inflammatory bowel disease and immune checkpoint inhibitor-associated colitis[82]. *Holdemanella biformis* is a well-characterised producer of SCFAs, particularly butyrate, and has been reported to exhibit both anti-inflammatory and anti-tumorigenic properties in the gut[83,84]. However, our analysis revealed a strong functional association with the L-tyrosine biosynthesis pathway, a metabolic pathway recently implicated in microbial adaptation to dietary fibre deficiency[85,86]. Importantly, increased L-tyrosine biosynthesis enhances microbial tyrosine fermentation, leading to elevated *p*-Cresol production[87]. This microbial metabolite is subsequently conjugated in the host to form uremic toxins such as *p*-Cresol sulphate and *p*-Cresol glucuronide, both of which have been implicated in systemic toxicity, chronic kidney disease[88,89], and elevated blood pressure in humans[85].

While these findings offer important insights, certain limitations cannot be overlooked, most notably, the small cohort size. The colonic quartiles were calculated based on transit time, not on geographical locations; thus, they represent proxy sites rather than the exact colonic regions we attempted to characterise. This underscores the need for novel technologies capable of capturing more precise, spatially resolved pH profiles across both luminal and tissue microenvironments. Following on from this, while faecal samples remain the most readily obtainable specimen for evaluating the human gut microbiome, they do not accurately reflect region-specific microbial communities; thus, such devices would also ideally enable

concurrent sampling of region-specific microbiome, facilitating a more integrated understanding of host–microbiome interactions within distinct gut niches. Therefore, our findings regarding quartile four regional colonic pH were not unexpected, as quartile four is most directly reflective of the rectum and, therefore, of the faecal microbiome from which metagenomic sequencing was performed. Nonetheless, our study has several strengths, including a similar representation of males and females and the use of an in vivo system to capture in detail the pH of the human GI tract. The device employed in this study is no longer commercially available, and no current alternatives offer comparable resolution or functionality. This renders our dataset both unique and timely, providing a valuable reference point for future investigations into gut physicochemical-immune axes in humans.

In conclusion, our findings reveal a physiologically significant axis linking gut microbial composition, colonic intraluminal pH, and the production of fibre-derived metabolites to systemic immune modulation in humans. This coordinated interplay demonstrates that local gut environmental cues, particularly those shaped by microbial fermentation and physicochemical gradients, can exert far-reaching effects on peripheral immune tone. These insights advance our understanding of how diet, microbial metabolism, and gut pH converge to regulate human immunity, with implications for the design of microbiome-targeted interventions in immune-mediated and inflammatory diseases.

Methods

The pH of Intestines and Blood-pressure Regulation (pHibre) cohort

The pH of Intestines and Blood-pressure Regulation (pHibre) study was approved by the Monash University Human Research Ethics Committee (Study ID: 23336) and followed the Declaration of Helsinki. All participants provided written consent. The study was registered with the Australian New Zealand Clinical Trials Registry under registration number ACTRN12620000284965. Recruitment of male and female volunteers was conducted between June 2020 and October 2021 through study advertisement. Inclusion criteria included body mass index (BMI) between 18.5–35 kg/m^2 and age between 18-70 years old. Exclusion criteria included non-English speaking; gastrointestinal disorders and diseases (including history of intestinal surgery, lactose intolerance, inflammatory bowel disease, celiac disease, chronic pancreatitis or other malabsorption disorder); gastrointestinal surgery in the last 3 months; type 1 or 2 diabetes; chronic kidney disease; swallowing disorders or severe dysphagia to food or pills; having implanted or portable electro-mechanical devices; and recent use of antibiotics (< 3 months) or probiotics (< 6 weeks). The recruitment summary is outlined in Figure 1A. Study outcomes are described in detail in the following sections and are summarised in Figure 1B. Briefly, the study included one visit where fasting blood glucose was measured (Table S1), followed by ingestion of the wireless pH-motility capsule (SmartPill) to measure transit time and pH[90]. The mean whole-gut transit time was 32.8 ± 17.6 hours. Participants also provided a faecal sample and self-assessed stool consistency using the Bristol Stool Form Scale (BSS)[91], with a median reported BSS stool classification of type 4 (Table S1).

Habitual dietary records

Participants completed a three-day food diary leading up to the appointment, on one weekend day, and on two weekdays to assess habitual intake. The dietary information was then analysed through a nutritional analysis software, FoodWorks 10 (Xyris, Queensland), using an Australian food composition database for energy, macro- and micronutrient intake (Table S1).

Wireless pH-motility (SmartPill) capsule data collection

Fasting participants were asked to eat a low-fat and low-fibre muesli bar, followed by ingestion of the SmartPill™ Motility Testing System (Medtronic). After being swallowed, the SmartPill™ measured in real-time, the intraluminal pH, pressure, and temperature as it travelled through the gastrointestinal tract. The information was transmitted wirelessly to a

portable receiver worn by the participants until excretion, indicated by a signal loss from the device coinciding with the passage of stools. GI transit times and pH data were independently determined from the Smart Pill™ data by at least two trained investigators.

Peripheral blood mononuclear cell (PBMC) isolation & flow cytometric preparation

PBMCs were isolated by density gradient centrifugation. Briefly, whole blood was diluted at a 1:1 volume ratio with Dulbecco's phosphate buffered saline (dPBS, 1X, Sigma-Aldrich, D8537) supplemented with 2% foetal bovine serum (FBS, Sigma-Aldrich, 12007C). The diluted blood was slowly overlayed onto Ficoll-Paque (GE Healthcare, 17-1440-03) at a 1:2 volume ratio to create an interface. Density gradient centrifugation was run at 700g (1800RPM) for 20 minutes at 20°C with the deceleration (brake) off. Following centrifugation, the plasma layer was aspirated, and the PBMC layer was harvested using a sterile transfer pipette. PBMCs were washed with cold 1x PBS and centrifuged at 400g (1400RPM) for 10 minutes. The cell pellet was then resuspended in 10ml of cold 1x PBS. Cell counts were performed manually using a haemocytometer and Trypan blue (0.4%; Invitrogen, T10282). Samples were cryopreserved until the time of the experiment. Briefly, isolated PBMCs were resuspended in freezing medium (10% DMSO; Sigma-Aldrich, D8418 and 90% FBS). Cryovials were then placed into a Mr. Frosty (ThermoFisher, 5100-0001) and into a -80°C freezer. Cryovials were transferred to liquid nitrogen storage the following day.

Frozen PBMC samples were retrieved, slowly thawed in a 37°C water bath and resuspended in pre-warmed RPMI 1640 (Biomedicine Learning and Teaching Building & Media Services Facility) supplemented with 10% FBS. Cells were centrifuged at 400g for 5 minutes. Cell counts were performed manually using a haemocytometer and Trypan blue (0.4%; Invitrogen, T10282). $2.5x10^6$ cells/mL per sample were stimulated with 50ng/mL phorbol 12-myristate 13-acetate (PMA; Sigma-Aldrich, 16561-29-8) and 1µg/mL ionomycin (Sigma-Aldrich, I0634) in a total of 3mL ($7.5x10^6$ cells total) and incubated at 5% CO2 at 37°C for 60 minutes. Cells were then treated with brefeldin A (5µg/mL, eBioscience™ Brefeldin A Solution (1000X), 00-4506-51) and monensin (5µg/mL, eBioscience™ Monensin Solution (1000X), 00-4505-51) and incubated for 5 hours and refrigerated overnight. Cells were washed and spun down at 400g for 5 minutes and $1x10^6$ viable cells per sample were subjected to flow cytometric staining. $1x10^6$ cells per sample were not subjected to the stimulation protocol to allow accurate staining and analysis of immune cell populations that are particularly sensitive to stimulation and at higher risk of cell death, such as neutrophils.

Flow cytometry

Cells were stained with ViaDye Red Fixable Viability Dye (1:500, Cytek Biosciences, R7-60008), incubated for 20 minutes at RT in the dark, washed with staining buffer, comprised of 1X dPBS supplemented with 2% bovine serum albumin (BSA, Sigma-Aldrich, A7906) and spun at 400g for 5 minutes at RT. Cells were blocked with True-Stain Monocyte Blocker (BioLegend, 426102) and diluted in Brilliant Stain Buffer Plus (BD Biosciences, 568264). The antibody panel designed incorporated a custom human immunoprofiling assay panel with 14 made-to-order cFluor reagents (Cytek Biosciences, RC-00685) and 15 externally sourced antibodies (Table S6). Surface antibodies TCRγδ and CCR7 were added to all stimulated samples, incubated for 10 minutes at RT in the dark, followed by the addition of all other surface antibody markers (Table S6). Unstimulated cells were incubated with a separate antibody cocktail containing CD14, CD15 and CD16 surface antibodies. Cells were incubated for 20 minutes at RT in the dark, washed with staining buffer and spun at 400g for 5 minutes at RT. Cells were fixed with the Foxp3/Transcription Factor Staining Buffer Kit (Sapphire Bioscience, TNB-0607-KIT), washed with 1X Perm Buffer, spun at 400g for 5 minutes at RT and at this time, unstimulated cells were ready for acquisition. Stimulated cells were stained with an antibody cocktail containing intracellular antibody markers as described in Table S6 for 60 minutes at RT. Samples were washed with 1X Perm Buffer, spun at 400g for 5 minutes at RT, and this time, stimulated cells were ready for acquisition. Samples were acquired on a Cytek Aurora 5 Laser Spectral Analyser at the FlowCore Facility of Monash University. Data was analysed using FlowJo v10.10.0, and gating strategies are outlined in Table S7.

Plasma short-chain fatty acid (SCFA) measurements

Fasting blood was collected in the morning, and plasma SCFAs were quantified using mass spectrometry as previously described[92]. Briefly, 20 µl of plasma was analysed in duplicates in a Q-Exactive Orbitrap mass spectrometer (Thermo Fisher Scientific) in conjunction with a Dionex UltiMate 3000 RS high-performance liquid chromatography (HPLC) system (Thermo Fisher Scientific). We accepted a coefficient of variability <15%. Standard curves were constructed using the area ratio of the target analyte, and the internal standard in the range of each analyte was used. The levels of butanoic and propionic acid in some samples were below detection level of the standard curve; in this case, they were considered half of the lowest measurable value (equivalent to 0.025 ng ml−1).

Faecal DNA extraction and high-throughput shotgun-metagenomic sequencing

The STORMS (Strengthening the Organization and Reporting of Microbiome Studies) reporting guidelines were followed throughout[93,94]. Participants collected stool samples at home in tubes containing DNA/RNA Shield (Zymo Research, R1100) for microbial DNA extraction. Tubes were brought to the clinics immediately or were stored at −20°C for less than 24 hours and then brought to the clinic, where they were stored at −80ºC until further processing. DNA was extracted using the DNeasy PowerSoil DNA isolation kit (Qiagen, 12888). Libraries were constructed using the Illumina DNA Prep (M) Tagmentation Kit (Illumina, 20018705) with IDT for Illumina DNA/RNA UD Index Sets A-D (Illumina, 20027213-16) according to the manufacturer's instructions, with a volume adjustment to accommodate processing in a 384-plate format. Resulting libraries were assessed using a high-sensitivity dsDNA fluorometric assay (QuantIT, ThermoFisher, Q33120) and individual libraries were visualised with capillary gel electrophoresis using the QIAxcel DNA High Resolution Kit (Qiagen, 929002). Libraries were required to meet minimum criteria for average size, smallest and largest fragment gating, and concentration. Individual libraries were pooled in equimolar amounts to create a sequencing pool, which was assessed using a high-sensitivity dsDNA fluorometric assay (QuantIT, ThermoFisher, Q33120) and visualised by capillary gel electrophoresis with the QIAxcel DNA High Resolution Kit (Qiagen, 929002). Pools were required to meet minimum criteria for average size, smallest and largest fragment gating, and concentration. Sequencing pools were loaded and sequenced on the Illumina NovaSeq™ 6000 using v1.5 300 bp PE sequencing reagents, according to the manufacturer's instructions, to a target depth of 3GB. Sequences were demultiplexed, sequencer adaptors were trimmed, and files were converted from bcl to fastq format. QC processing of raw stool shotgun-metagenomic forward and reverse reads in fastq format was performed using KneadData7 as a wrapper. Raw reads were initially quality trimmed to remove base calls with a Phred score lower than 33 and a minimum read length of 50 nucleotides (SLIDINGWINDOW:4:20 MINLEN:50) using Trimmomatic v0.38.8 Trimmed reads were then host-filtered if they mapped against the human (GRCh37 and GRCh38) or the Escherichia phage phiX174 (NCBI accession: NC_001422) genomes using Bowtie29 v.2.3.5 very-sensitive pre-set parameters (-D 20 -R 3 -N 0 -L 20 -i S,1,0.50). QC visualisation was performed with fastQC v.0.12.1 and multiQC10 v1.19.

Microbial taxonomic and functional profiling

Taxonomic profiling per sample was performed using MetaPhlAn11 v4.1 and the mpa_vJun23_CHOCOPhlAnSGB_202307 database, which spans 36,822 species-level genome bins (SGB) for bacteria, archaea, and eukaryote, relying on over 5 million unique clade-specific marker genes. The CHOCOPhlAn database leverages systematically organised and annotated microbial genomes and gene family clusters based on the NCBI and UniProt/UniRef reference databases. For taxonomic profiling, by default, MetaPhlAn searched for high-quality reads matching at least 20% of the unique clade-specific marker genes available for a species using nucleotide BLAST (blastn) with an e-value (the number of alignments expected by chance) threshold of $1x10^{-6}$, indicating a strong similarity between the query sequence and the subject sequence in the database. When multiple matches occurred between a read and markers from different clades, only the top hit was considered, in a way that a read could only be mapped to a single clade. The obtained reads per kilobase (RPK) were normalised by the total number of reads per sample in the metagenome to ensure fair comparisons of abundances across samples. Abundance per sample was calculated based on the coverage of the species-specific marker genes multiplied by the clade's average genome size. Relative abundances were then calculated as local clade abundance divided by the sum of all the local abundances for that sample.

Functional read profiling was performed using HUMAnN7 v3.9, with default settings. For functional profiling, HUMAnN uses Bowtie29 (for sequence alignment to pangenomes), Prodigal12 (for ORF identification), and Diamond13 (for BLAST local sequence alignment) against the UniProt Reference Clusters database at 90% identity (UniRef90). The abundances of metaCyc14 pathways were obtained from total coverage depth (RPK) values per sample, which were then normalised to relative abundances to enable comparisons between samples with different sequencing depths. Reads that mapped to gene families but could not be assigned to any known metaCyc pathway were grouped as 'unintegrated', whereas reads that did not map to any gene family were categorised as 'unmapped'. These were excluded before functional differential abundance analyses.

Microbial and metabolic pathway differential abundance analyses

Differential abundance analyses were conducted using the R package MaAsLin216 (v1.15.1) at both the species and pathway levels, employing linear regressions adjusted for age, sex, and BMI. Relative abundances were normalised using the centred log-ratio (CLR) method and used

as input. Species were included if present in at least one individual in the sample (totalling 1678 species). Additionally, metaCyc pathways were analysed at the species level, as provided by the HuManN pipeline and were included if present in at least one individual (totalling 15,173 species-level metaCyc pathways). Variables demonstrating fewer than two significant associations were omitted.

Colonic pH diversity metrics analysis

Both α and β diversity metrics were calculated from colonic minimum, median, and maximum pH values, as well as quartile pH data. Specifically, α diversity, which estimates species diversity within a sample, was calculated using the Shannon and Simpson indices using the microbiome R package. β diversity was calculated based on both unweighted and weighted UniFrac metrics, using the rbiom R package and the Species Genome Bin (SGB) phylogenetic tree version mpa_vJun23_CHOCOPhlAnSGB_202307.nwk provided by MetaPhlAn v4.1.

Statistical analyses

All statistical analyses were conducted in R 4.3.2. Normality was assessed using the Shapiro-Wilk test. To minimise the influence of extreme values, outliers were removed using the interquartile range (IQR) method. For each variable, the first quartile (Q1) and third quartile (Q3) were calculated, and the IQR was defined as the difference between Q3 and Q1. Data points falling below Q1 – 1.5 × IQR or above Q3 + 1.5 × IQR were excluded from further analysis. Comparisons between quartiles were performed using a one-way analysis of variance (ANOVA) followed by pairwise t-tests. Data presented as mean ± standard error of mean (SEM). Spearman's rank correlations were performed on non-normally distributed continuous variables. A significance threshold of $P<0.05$ was used. Adjustments were performed using the Benjamini–Hochberg False FDR method, and $q<0.05$ was considered statistically significant. For alpha diversity, linear regressions (on log-transformed α metrics) were used for continuous variables. For beta diversity, Permutational multivariate analyses of variance (PERMANOVA) using 9,999 permutations were conducted with the adonis2 function from the vegan15 R package.

Data Availability

Microbiome data are available at https://doi.org/10.5281/zenodo.17645792. We did not obtain patient consent for all the data to be made publicly available. However, the data underlying this article can be shared for selected research questions upon reasonable request to the corresponding author. Please email F.Z.M. at francine.marques@monash.edu, who will respond within 4 weeks.

Code Availability

The codes supporting this study's findings are available from the corresponding author. Please email F.Z.M. at francine.marques@monash.edu.

Acknowledgements

This study was supported by a National Heart Foundation Vanguard Grant (102927) and a National Health & Medical Research Council of Australia (NHMRC) Ideas Grant (GTN2017382). F.Z.M. is supported by a Senior Medical Research Fellowship from the Sylvia and Charles Viertel Charitable Foundation, a National Heart Foundation Future Leader Fellowship (105663), and National Health & Medical Research Council (NHMRC) Emerging Leader Fellowship (GNT2017382). J.A.O. is supported by a NHMRC Fellowship (GNT1124288). S.J.T is supported by NHMRC Ideas Grant (GTN2037610). The authors thank Monash University FlowCore, the Monash Statistical Consulting Service, the Monash eResearch capabilities for providing access to M3 servers, and the Australian Genome Research Facility. The authors also thank Dr Matthew Snelson and Michael Nakai for their guided assistance with data analysis tools and experimental work respectively.

Contributions

E.D. designed, planned and performed the human immunoprofiling flow cytometry experiment, data analyses, and wrote the manuscript. D.R.J. secured human ethics approval, recruited the participants, and analysed the SmartPill™ data, verified by C.K.Y and D.S.. L.C.T. and C.Y. contributed to analysis tools and data analysis. D.A. and D.C. measured SCFAs. P.R.G. contributed to the interpretation of intestinal pH. C.R.M. contributed towards the central hypothesis and securing funding. J.O.D. provided intellectual input and assisted in the planning and execution of the human immunoprofiling flow cytometry experiment. J.M. contributed towards trial design, supervision, and data collection and analysis. F.Z.M. conceived and designed the study, secured funding, provided intellectual input and contributed

to writing the article. All authors approved of and contributed to the final version of the manuscript.

References

1. Fallingborg J. Intraluminal pH of the human gastrointestinal tract. *Dan Med Bull*. 1999;46:183-196.
2. Evans DF, Pye G, Bramley R, Clark AG, Dyson TJ, Hardcastle JD. Measurement of gastrointestinal pH profiles in normal ambulant human subjects. *Gut*. 1988;29:1035-1041. doi: 10.1136/gut.29.8.1035
3. Koziolek M, Grimm M, Becker D, Iordanov V, Zou H, Shimizu J, Wanke C, Garbacz G, Weitschies W. Investigation of pH and temperature profiles in the GI tract of fasted human subjects using the Intellicap® system. *Journal of pharmaceutical sciences*. 2015;104:2855-2863.
4. Maurer JM, Schellekens RC, van Rieke HM, Wanke C, Iordanov V, Stellaard F, Wutzke KD, Dijkstra G, van der Zee M, Woerdenbag HJ, et al. Gastrointestinal pH and Transit Time Profiling in Healthy Volunteers Using the IntelliCap System Confirms Ileo-Colonic Release of ColoPulse Tablets. *PLoS One*. 2015;10:e0129076. doi: 10.1371/journal.pone.0129076
5. Hooper LV, Wong MH, Thelin A, Hansson L, Falk PG, Gordon JI. Molecular analysis of commensal host-microbial relationships in the intestine. *Science*. 2001;291:881-884.
6. Zoetendal EG, von Wright A, Vilpponen-Salmela T, Ben-Amor K, Akkermans AD, de Vos WM. Mucosa-associated bacteria in the human gastrointestinal tract are uniformly distributed along the colon and differ from the community recovered from feces. *Applied and environmental microbiology*. 2002;68:3401-3407.
7. Dieterich W, Schink M, Zopf Y. Microbiota in the Gastrointestinal Tract. *Med Sci (Basel)*. 2018;6. doi: 10.3390/medsci6040116
8. Mowat AM, Agace WW. Regional specialization within the intestinal immune system. *Nat Rev Immunol*. 2014;14:667-685. doi: 10.1038/nri3738
9. Sekirov I, Russell SL, Antunes LCM, Finlay BB. Gut Microbiota in Health and Disease. *Physiological Reviews*. 2010;90:859-904. doi: 10.1152/physrev.00045.2009
10. Cummings JH, Pomare EW, Branch WJ, Naylor CP, Macfarlane GT. Short chain fatty acids in human large intestine, portal, hepatic and venous blood. *Gut*. 1987;28:1221-1227. doi: 10.1136/gut.28.10.1221
11. Campbell JM, Fahey Jr GC, Wolf BW. Selected indigestible oligosaccharides affect large bowel mass, cecal and fecal short-chain fatty acids, pH and microflora in rats. *The Journal of nutrition*. 1997;127:130-136.
12. Duncan SH, Louis P, Thomson JM, Flint HJ. The role of pH in determining the species composition of the human colonic microbiota. *Environ Microbiol*. 2009;11:2112-2122. doi: 10.1111/j.1462-2920.2009.01931.x
13. Xie Z, He W, Gobbi A, Bertram HC, Nielsen DS. The effect of in vitro simulated colonic pH gradients on microbial activity and metabolite production using common prebiotics as substrates. *BMC Microbiology*. 2024;24:83. doi: 10.1186/s12866-024-03235-2
14. Scott KP, Gratz SW, Sheridan PO, Flint HJ, Duncan SH. The influence of diet on the gut microbiota. *Pharmacological Research*. 2013;69:52-60. doi: https://doi.org/10.1016/j.phrs.2012.10.020
15. Cummings JH. Short chain fatty acids in the human colon. *Gut*. 1981;22:763.
16. Xie L, Muralitharan RR, Dinakis E, Antonacci S, Leung KC, McArdle Z, Mirabito Colafella K, Nakai M, Paterson M, Peh A, et al. Dietary fibre controls blood pressure and cardiovascular risk by lowering large intestinal pH and activating the proton-

sensing receptor GPR65. *bioRxiv*. 2025:2022.2011.2017.516695. doi: 10.1101/2022.11.17.516695
17. Pabst R, Russell MW, Brandtzaeg P. Tissue distribution of lymphocytes and plasma cells and the role of the gut. *Trends in immunology*. 2008;29:206-208.
18. Macpherson AJ, Harris NL. Interactions between commensal intestinal bacteria and the immune system. *Nature Reviews Immunology*. 2004;4:478-485.
19. Bauer H, Horowitz RE, Levenson SM, Popper H. The response of the lymphatic tissue to the microbial flora. Studies on germfree mice. *The American journal of pathology*. 1963;42:471.
20. Macpherson AJ, Hunziker L, McCoy K, Lamarre A. IgA responses in the intestinal mucosa against pathogenic and non-pathogenic microorganisms. *Microbes Infect*. 2001;3:1021-1035. doi: 10.1016/s1286-4579(01)01460-5
21. Helgeland L, Vaage JT, Rolstad B, Midtvedt T, Brandtzaeg P. Microbial colonization influences composition and T-cell receptor V beta repertoire of intraepithelial lymphocytes in rat intestine. *Immunology*. 1996;89:494-501. doi: 10.1046/j.1365-2567.1996.d01-783.x
22. El Aidy S, van Baarlen P, Derrien M, Lindenbergh-Kortleve DJ, Hooiveld G, Levenez F, Doré J, Dekker J, Samsom JN, Nieuwenhuis EE, et al. Temporal and spatial interplay of microbiota and intestinal mucosa drive establishment of immune homeostasis in conventionalized mice. *Mucosal Immunol*. 2012;5:567-579. doi: 10.1038/mi.2012.32
23. Round JL, Mazmanian SK. The gut microbiota shapes intestinal immune responses during health and disease. *Nature Reviews Immunology*. 2009;9:313-323. doi: 10.1038/nri2515
24. Roager HM, Hansen L, Bahl MI, Frandsen HL, Carvalho V, Gøbel RJ, Dalgaard MD, Plichta DR, Sparholt MH, Vestergaard H. Colonic transit time is related to bacterial metabolism and mucosal turnover in the gut. *Nature microbiology*. 2016;1:1-9.
25. Gill SK, Rossi M, Bajka B, Whelan K. Dietary fibre in gastrointestinal health and disease. *Nature Reviews Gastroenterology & Hepatology*. 2021;18:101-116. doi: 10.1038/s41575-020-00375-4
26. Mueller SN, Ahmed R. High antigen levels are the cause of T cell exhaustion during chronic viral infection. *Proceedings of the National Academy of Sciences*. 2009;106:8623-8628.
27. Wherry EJ. T cell exhaustion. *Nature immunology*. 2011;12:492-499.
28. Jin H-T, Anderson AC, Tan WG, West EE, Ha S-J, Araki K, Freeman GJ, Kuchroo VK, Ahmed R. Cooperation of Tim-3 and PD-1 in CD8 T-cell exhaustion during chronic viral infection. *Proceedings of the National Academy of Sciences*. 2010;107:14733-14738.
29. Fourcade J, Sun Z, Benallaoua M, Guillaume P, Luescher IF, Sander C, Kirkwood JM, Kuchroo V, Zarour HM. Upregulation of Tim-3 and PD-1 expression is associated with tumor antigen–specific CD8+ T cell dysfunction in melanoma patients. *Journal of Experimental Medicine*. 2010;207:2175-2186.
30. Fuller MJ, Khanolkar A, Tebo AE, Zajac AJ. Maintenance, loss, and resurgence of T cell responses during acute, protracted, and chronic viral infections. *The Journal of Immunology*. 2004;172:4204-4214.
31. Cravedi P, Li XC. Interleukin-2 and PD-1 synergistically modify T cell exhaustion programs. *American Journal of Transplantation*. 2023;23:161-162. doi: 10.1016/j.ajt.2023.01.002
32. Legat A, Speiser DE, Pircher H, Zehn D, Fuertes Marraco SA. Inhibitory Receptor Expression Depends More Dominantly on Differentiation and Activation than

"Exhaustion" of Human CD8 T Cells. *Frontiers in Immunology*. 2013;Volume 4 - 2013. doi: 10.3389/fimmu.2013.00455
33. Mazet JM, Mahale JN, Tong O, Watson RA, Lechuga-Vieco AV, Pirgova G, Lau VWC, Attar M, Koneva LA, Sansom SN, et al. IFNγ signaling in cytotoxic T cells restricts anti-tumor responses by inhibiting the maintenance and diversity of intra-tumoral stem-like T cells. *Nature Communications*. 2023;14:321. doi: 10.1038/s41467-023-35948-9
34. Baxter AE, Kaufmann DE. Tumor-necrosis factor is a master of T cell exhaustion. *Nature Immunology*. 2016;17:476-478. doi: 10.1038/ni.3436
35. Guo Z, Zhang J, Wang Z, Ang KY, Huang S, Hou Q, Su X, Qiao J, Zheng Y, Wang L, et al. Intestinal Microbiota Distinguish Gout Patients from Healthy Humans. *Sci Rep*. 2016;6:20602. doi: 10.1038/srep20602
36. De Maesschalck C, Van Immerseel F, Eeckhaut V, De Baere S, Cnockaert M, Croubels S, Haesebrouck F, Ducatelle R, Vandamme P. Faecalicoccus acidiformans gen. nov., sp. nov., isolated from the chicken caecum, and reclassification of Streptococcus pleomorphus (Barnes et al. 1977), Eubacterium biforme (Eggerth 1935) and Eubacterium cylindroides (Cato et al. 1974) as Faecalicoccus pleomorphus comb. nov., Holdemanella biformis gen. nov., comb. nov. and Faecalitalea cylindroides gen. nov., comb. nov., respectively, within the family Erysipelotrichaceae. *International Journal of Systematic and Evolutionary Microbiology*. 2014;64:3877-3884.
37. Lozupone Catherine A, Li M, Campbell Thomas B, Flores Sonia C, Linderman D, Gebert Matthew J, Knight R, Fontenot Andrew P, Palmer Brent E. Alterations in the Gut Microbiota Associated with HIV-1 Infection. *Cell Host & Microbe*. 2013;14:329-339. doi: 10.1016/j.chom.2013.08.006
38. Zinkernagel RM, Doherty PC. Restriction of in vitro T cell-mediated cytotoxicity in lymphocytic choriomeningitis within a syngeneic or semiallogeneic system. *Nature*. 1974;248:701-702. doi: 10.1038/248701a0
39. Mittrücker H-W, Visekruna A, Huber M. Heterogeneity in the Differentiation and Function of CD8+ T Cells. *Archivum Immunologiae et Therapiae Experimentalis*. 2014;62:449-458. doi: 10.1007/s00005-014-0293-y
40. Bachem A, Makhlouf C, Binger KJ, de Souza DP, Tull D, Hochheiser K, Whitney PG, Fernandez-Ruiz D, Dähling S, Kastenmüller W, et al. Microbiota-Derived Short-Chain Fatty Acids Promote the Memory Potential of Antigen-Activated CD8⁺ T Cells. *Immunity*. 2019;51:285-297.e285. doi: 10.1016/j.immuni.2019.06.002
41. Kim MT, Harty JT. Impact of Inflammatory Cytokines on Effector and Memory CD8+ T Cells. *Frontiers in Immunology*. 2014;Volume 5 - 2014. doi: 10.3389/fimmu.2014.00295
42. Bachem A, Clarke M, Kong G, Tarasova I, Dryburgh L, Kosack L, Lee AR, Newland LD, Wagner T, Bawden E, et al. Microbiota-derived butyrate promotes a FOXO1-induced stemness program and preserves CD8(+) T cell immunity against melanoma. *Immunity*. 2025;58:2799-2813.e2798. doi: 10.1016/j.immuni.2025.10.004
43. Rodrigues LS, Barreto AS, Bomfim LGS, Gomes MC, Ferreira NLC, da Cruz GS, Magalhães LS, de Jesus AR, Palatnik-de-Sousa CB, Corrêa CB, et al. Multifunctional, TNF-α and IFN-γ-Secreting CD4 and CD8 T Cells and CD8High T Cells Are Associated With the Cure of Human Visceral Leishmaniasis. *Frontiers in Immunology*. 2021;Volume 12 - 2021. doi: 10.3389/fimmu.2021.773983
44. Mace TA, Zhong L, Kokolus KM, Repasky EA. Effector CD8+ T cell IFN-γ production and cytotoxicity are enhanced by mild hyperthermia. *International Journal of Hyperthermia*. 2012;28:9-18. doi: 10.3109/02656736.2011.616182

45. Montfort A, Colacios C, Levade T, Andrieu-Abadie N, Meyer N, Ségui B. The TNF paradox in cancer progression and immunotherapy. *Frontiers in immunology*. 2019;10:1818.
46. Jiang Y, Li Y, Zhu B. T-cell exhaustion in the tumor microenvironment. *Cell Death & Disease*. 2015;6:e1792-e1792. doi: 10.1038/cddis.2015.162
47. Alexander MR, Dale BL, Smart CD, Elijovich F, Wogsland CE, Lima SM, Irish JM, Madhur MS. Immune Profiling Reveals Decreases in Circulating Regulatory and Exhausted T Cells in Human Hypertension. *JACC Basic Transl Sci*. 2023;8:319-336. doi: 10.1016/j.jacbts.2022.09.007
48. Naffah de Souza C, Breda LCD, Khan MA, Almeida SRd, Câmara NOS, Sweezey N, Palaniyar N. Alkaline pH Promotes NADPH Oxidase-Independent Neutrophil Extracellular Trap Formation: A Matter of Mitochondrial Reactive Oxygen Species Generation and Citrullination and Cleavage of Histone. *Frontiers in Immunology*. 2018;Volume 8 - 2017. doi: 10.3389/fimmu.2017.01849
49. Qiu Z, Huang C, Xu C, Xu Y. Predictive role of neutrophil-to-lymphocyte ratio in metabolic syndrome: Meta-analysis of 70,937 individuals. *BMC Endocrine Disorders*. 2024;24:155. doi: 10.1186/s12902-024-01689-z
50. Ayeni FA, Biagi E, Rampelli S, Fiori J, Soverini M, Audu HJ, Cristino S, Caporali L, Schnorr SL, Carelli V. Infant and adult gut microbiome and metabolome in rural Bassa and urban settlers from Nigeria. *Cell reports*. 2018;23:3056-3067.
51. Barrett HL, Gomez-Arango LF, Wilkinson SA, McIntyre HD, Callaway LK, Morrison M, Dekker Nitert M. A vegetarian diet is a major determinant of gut microbiota composition in early pregnancy. *Nutrients*. 2018;10:890.
52. Mueller S, Saunier K, Hanisch C, Norin E, Alm L, Midtvedt T, Cresci A, Silvi S, Orpianesi C, Verdenelli MC. Differences in fecal microbiota in different European study populations in relation to age, gender, and country: a cross-sectional study. *Applied and environmental microbiology*. 2006;72:1027-1033.
53. Das B, Ghosh TS, Kedia S, Rampal R, Saxena S, Bag S, Mitra R, Dayal M, Mehta O, Surendranath A. Analysis of the gut microbiome of rural and urban healthy Indians living in sea level and high altitude areas. *Scientific reports*. 2018;8:10104.
54. Obregon-Tito AJ, Tito RY, Metcalf J, Sankaranarayanan K, Clemente JC, Ursell LK, Zech Xu Z, Van Treuren W, Knight R, Gaffney PM. Subsistence strategies in traditional societies distinguish gut microbiomes. *Nature communications*. 2015;6:6505.
55. Turpin W, Espin-Garcia O, Xu W, Silverberg MS, Kevans D, Smith MI, Guttman DS, Griffiths A, Panaccione R, Otley A. Association of host genome with intestinal microbial composition in a large healthy cohort. *Nature genetics*. 2016;48:1413-1417.
56. Pátek M. Branched-chain amino acids. In: *Amino Acid Biosynthesis~ Pathways, Regulation and Metabolic Engineering*. Springer; 2007:129-162.
57. Chen X-h, Liu S-r, Peng B, Li D, Cheng Z-x, Zhu J-x, Zhang S, Peng Y-m, Li H, Zhang T-t, et al. Exogenous l-Valine Promotes Phagocytosis to Kill Multidrug-Resistant Bacterial Pathogens. *Frontiers in Immunology*. 2017;Volume 8 - 2017. doi: 10.3389/fimmu.2017.00207
58. Turvey SE, Broide DH. Innate immunity. *Journal of Allergy and Clinical Immunology*. 2010;125:S24-S32. doi: https://doi.org/10.1016/j.jaci.2009.07.016
59. Covarrubias AJ, Aksoylar HI, Horng T. Control of macrophage metabolism and activation by mTOR and Akt signaling. Paper/Poster presented at: Seminars in immunology; 2015;

60. Yeo JC, Wall AA, Luo L, Stow JL. Rab31 and APPL2 enhance FcγR-mediated phagocytosis through PI3K/Akt signaling in macrophages. *Molecular biology of the cell*. 2015;26:952-965.
61. Schmidl C, Renner K, Peter K, Eder R, Lassmann T, Balwierz PJ, Itoh M, Nagao-Sato S, Kawaji H, Carninci P. Transcription and enhancer profiling in human monocyte subsets. *Blood, The Journal of the American Society of Hematology*. 2014;123:e90-e99.
62. Thandapani P, Kloetgen A, Witkowski MT, Glytsou C, Lee AK, Wang E, Wang J, LeBoeuf SE, Avrampou K, Papagiannakopoulos T, et al. Valine tRNA levels and availability regulate complex I assembly in leukaemia. *Nature*. 2022;601:428-433. doi: 10.1038/s41586-021-04244-1
63. Cameron J, Moro F, Simmonds H. Gout, uric acid and purine metabolism in paediatric nephrology. *Pediatric Nephrology*. 1993;7:105-118.
64. Schlesinger N. Dietary factors and hyperuricaemia. *Current pharmaceutical design*. 2005;11:4133-4138.
65. So A, Thorens B. Uric acid transport and disease. *The Journal of clinical investigation*. 2010;120:1791-1799.
66. Braga TT, Forni MF, Correa-Costa M, Ramos RN, Barbuto JA, Branco P, Castoldi A, Hiyane MI, Davanso MR, Latz E, et al. Soluble Uric Acid Activates the NLRP3 Inflammasome. *Scientific Reports*. 2017;7:39884. doi: 10.1038/srep39884
67. Shi Y, Evans JE, Rock KL. Molecular identification of a danger signal that alerts the immune system to dying cells. *Nature*. 2003;425:516-521.
68. Yamaoka T, Yano M, Kondo M, Sasaki H, Hino S, Katashima R, Moritani M, Itakura M. Feedback inhibition of amidophosphoribosyltransferase regulates the rate of cell growth via purine nucleotide, DNA, and protein syntheses. *Journal of Biological Chemistry*. 2001;276:21285-21291.
69. Webb R, Jeffries M, Sawalha AH. Uric acid directly promotes human T-cell activation. *The American journal of the medical sciences*. 2009;337:23-27.
70. Pérez-Mazliah D, Albareda MC, Alvarez MG, Lococo B, Bertocchi GL, Petti M, Viotti RJ, Laucella SA. Allopurinol reduces antigen-specific and polyclonal activation of human T cells. *Front Immunol*. 2012;3:295. doi: 10.3389/fimmu.2012.00295
71. Katsuyama T, Tsokos GC, Moulton VR. Aberrant T cell signaling and subsets in systemic lupus erythematosus. *Frontiers in immunology*. 2018;9:1088.
72. Ishida Y, Agata Y, Shibahara K, Honjo T. Induced expression of PD-1, a novel member of the immunoglobulin gene superfamily, upon programmed cell death. *The EMBO journal*. 1992;11:3887-3895.
73. Okazaki T, Honjo T. PD-1 and PD-1 ligands: from discovery to clinical application. *International immunology*. 2007;19:813-824.
74. Śledzińska A, Menger L, Bergerhoff K, Peggs KS, Quezada SA. Negative immune checkpoints on T lymphocytes and their relevance to cancer immunotherapy. *Molecular oncology*. 2015;9:1936-1965.
75. Dong Y, Sun Q, Zhang X. PD-1 and its ligands are important immune checkpoints in cancer. *Oncotarget*. 2016;8:2171.
76. Zhu X, Li K, Liu G, Wu R, Zhang Y, Wang S, Xu M, Lu L, Li P. Microbial metabolite butyrate promotes anti-PD-1 antitumor efficacy by modulating T cell receptor signaling of cytotoxic CD8 T cell. *Gut Microbes*. 2023;15:2249143. doi: 10.1080/19490976.2023.2249143
77. Luu M, Weigand K, Wedi F, Breidenbend C, Leister H, Pautz S, Adhikary T, Visekruna A. Regulation of the effector function of CD8(+) T cells by gut microbiota-

derived metabolite butyrate. *Sci Rep*. 2018;8:14430. doi: 10.1038/s41598-018-32860-x
78. Vardhana SA, Hwee MA, Berisa M, Wells DK, Yost KE, King B, Smith M, Herrera PS, Chang HY, Satpathy AT, et al. Impaired mitochondrial oxidative phosphorylation limits the self-renewal of T cells exposed to persistent antigen. *Nature Immunology*. 2020;21:1022-1033. doi: 10.1038/s41590-020-0725-2
79. Bedoui S, Binger K, Kallies A, Turner SJ, McConville M, Gebhardt T, Bachem A. Microbiota-derived butyrate promotes cellular metabolism and memory potential of antigen-activated CD8+ T cells. *The Journal of Immunology*. 2019;202:189.181-189.181. doi: 10.4049/jimmunol.202.Supp.189.1
80. Vinolo MAR, Ferguson GJ, Kulkarni S, Damoulakis G, Anderson K, Bohlooly-Y M, Stephens L, Hawkins PT, Curi R. SCFAs Induce Mouse Neutrophil Chemotaxis through the GPR43 Receptor. *PLOS ONE*. 2011;6:e21205. doi: 10.1371/journal.pone.0021205
81. Li G, Lin J, Zhang C, Gao H, Lu H, Gao X, Zhu R, Li Z, Li M, Liu Z. Microbiota metabolite butyrate constrains neutrophil functions and ameliorates mucosal inflammation in inflammatory bowel disease. *Gut Microbes*. 2021;13:1968257. doi: 10.1080/19490976.2021.1968257
82. Wang W, Yu Y, Wang R, Wang Y, Ding X, Lu G, Lu C, Liang C, Zhang S, Yi B, et al. Holdemanella biformis augments washed microbiota transplantation for the treatment of radiation enteritis. *Gut*. 2025:gutjnl-2025-335230. doi: 10.1136/gutjnl-2025-335230
83. Zagato E, Pozzi C, Bertocchi A, Schioppa T, Saccheri F, Guglietta S, Fosso B, Melocchi L, Nizzoli G, Troisi J. Endogenous murine microbiota member Faecalibaculum rodentium and its human homologue protect from intestinal tumour growth. *Nature microbiology*. 2020;5:511-524.
84. Pujo J, Petitfils C, Le Faouder P, Eeckhaut V, Payros G, Maurel S, Perez-Berezo T, Van Hul M, Barreau F, Blanpied C. Bacteria-derived long chain fatty acid exhibits anti-inflammatory properties in colitis. *Gut*. 2021;70:1088-1097.
85. Xu C, Xie L, Barlow CK, Tavares LC, Dinakis E, Louca P, Moustafa JE-S, Yang C, Nakai M, Wang X, et al. Lack of dietary fibre increases gut microbiome-derived uremic toxins that contribute to increased blood pressure. *medRxiv*. 2025:2025.2009.2016.25335853. doi: 10.1101/2025.09.16.25335853
86. Birkett A, Muir J, Phillips J, Jones G, O'Dea K. Resistant starch lowers fecal concentrations of ammonia and phenols in humans. *The American Journal of Clinical Nutrition*. 1996;63:766-772.
87. Bone E, Tamm A, Hill M. The production of urinary phenols by gut bacteria and their possible ce: role in the causation of large bowel cancer. *The American journal of clinical nutrition*. 1976;29:1448-1454.
88. Liabeuf S, Barreto DV, Barreto FC, Meert N, Glorieux G, Schepers E, Temmar M, Choukroun G, Vanholder R, Massy ZA. Free p-cresylsulphate is a predictor of mortality in patients at different stages of chronic kidney disease. *Nephrology Dialysis Transplantation*. 2010;25:1183-1191.
89. Nigam SK, Bush KT. Uraemic syndrome of chronic kidney disease: altered remote sensing and signalling. *Nature Reviews Nephrology*. 2019;15:301-316.
90. Diaz Tartera HO, Webb DL, Al-Saffar AK, Halim MA, Lindberg G, Sangfelt P, Hellström PM. Validation of SmartPill® wireless motility capsule for gastrointestinal transit time: Intra-subject variability, software accuracy and comparison with video capsule endoscopy. *Neurogastroenterology & Motility*. 2017;29:e13107. doi: https://doi.org/10.1111/nmo.13107

91. Lewis SJ, Heaton KW. Stool form scale as a useful guide to intestinal transit time. *Scandinavian journal of gastroenterology*. 1997;32:920-924.
92. Jama H, Dona MSI, Dinakis E, Nakai M, Paterson MR, Shihata W, Krstevski C, Cohen CD, Weeks KL, Farrugia GE, et al. Maternal diet and gut microbiota influence predisposition to cardiovascular disease in the offspring. *bioRxiv*. 2022:2022.2003.2012.480450. doi: 10.1101/2022.03.12.480450
93. Marques FZ, Jama HA, Tsyganov K, Gill PA, Rhys-Jones D, Muralitharan RR, Muir J, Holmes A, Mackay CR. Guidelines for Transparency on Gut Microbiome Studies in Essential and Experimental Hypertension. *Hypertension*. 2019;74:1279-1293. doi: 10.1161/hypertensionaha.119.13079
94. Mirzayi C, Renson A, Zohra F, Elsafoury S, Geistlinger L, Kasselman LJ, Eckenrode K, van de Wijgert J, Loughman A, Marques FZ, et al. Reporting guidelines for human microbiome research: the STORMS checklist. *Nat Med*. 2021;27:1885-1892. doi: 10.1038/s41591-021-01552-x
95. Macfarlane GT, Gibson GR, Cummings JH. Comparison of fermentation reactions in different regions of the human colon. *J Appl Bacteriol*. 1992;72:57-64. doi: 10.1111/j.1365-2672.1992.tb04882.x

Figure legends

Figure 1. Recruitment and cohort characteristics. (A) Recruitment summary of the pH of Intestines and Blood-pressure Regulation (pHibre) study; out of 91 expressions of interest, 54 participants finished the trial. **(B)** Data collection strategies, methods, and analyses of participants' dietary habits, SmartPill outcomes, and downstream whole-blood and faecal analyses are summarised. Figures were created on BioRender. GI, gastrointestine; COVID-19, coronavirus disease; BMI, body mass index.

Figure 2. Colonic pH and associations with immune cells, dietary fibre and short-chain fatty acids (SCFAs). (A) Graphic scheme of the regional pH profile in the colon and respective bacterial activity and SCFA concentration, adapted from[10,95] and created on BioRender. **(B)** Regional pH profile in the colon of the pHibre cohort generated by the SmartPill. **(C-J)** Spearman's rank correlations between colonic minimum, median and maximum pH and quartile data. Spearman's rank correlations as heatmaps between **(K)** colonic pH variables and transit time, diet, plasma SCFAs and immune cell populations/sub-types, and between **(L)** plasma SCFA levels, immune cell populations/sub-types and diet. Comparisons between quartiles were performed using a one-way analysis of variance (ANOVA) followed by pairwise t-tests. Data presented as mean ± standard error of mean (SEM). Spearman's rank correlations were performed on non-normally distributed continuous variables. The colour gradient represents the strength and direction of correlation (red = positive, blue = negative). Adjustments were performed using the Benjamini–Hochberg False FDR method. Raw unadjusted P-values are presented in heatmaps; *P<0.05, **P<0.01. n=41-54. CTT, colonic transit time; GET, gastrointestinal emptying time; SLBTT, small and large bowel transit time; WGTT, whole gut transit time; SCFA, short-chain fatty acid; CM, central memory; TEMRA, terminally differentiated effector memory T cells; IFN-γ, interferon- γ; NK, natural killer; TNF-α, tumour necrosis factor- α; IL-, interleukin-; EM, effector memory; T regs, T regulatory cells; PD-1, programmed cell death protein 1.

Figure 3. Associations between colonic pH, immune cells, the gut microbiome and species-specific metabolic pathways. Differentially abundant associations between **(A)** colonic pH in the fourth quartile (Q4) and species-specific metabolic pathways (grouped by function), **(B)**

immune cell populations/sub-types (grouped into categories) and species (grouped by genus) and **(C)** immune cell populations/sub-types (grouped into categories) and species-specific metabolic pathways (grouped by function). Only significant associations (q<0.05) with two or more associations are depicted in the chord diagrams. Line thickness is scaled to the significance of the association (−log10(FDR)). Figures were generated with the circlize R package (v0.4.16). n=48-53.

Figure 4. Associations between Holdemanella biformis and its pathways with the systemic immune system. Differentially abundant associations between the bacterial species Holdemanella biformis and **(A)** immune cell populations/sub-types, and **(B)** metabolic pathways. Only significant associations (q<0.05) are depicted. In panel A, coefficient of enrichment (β) quantifies the direction and strength of the association, with standard errors (SE) shown as horizontal error bars. In panel B, the size of the points corresponds to the significance of the association (−log10(FDR)), and the point colour intensity reflects the scaled effect size (coefficient, β), with stronger colours indicating larger effect sizes. Immune cell types in bold overlap in both analyses. Figures were generated with the ggplot2 R package (v3.5.2). n=48-53. IL-, interleukin-; PD-1, programmed cell death protein 1; HLA-DR, human leukocyte antigen-DR isotype; PMDSCs, polymorphonuclear myeloid-derived suppressor cells; TNF-α, tumour necrosis factor- α; NK, natural killer.

Figure 5. Eubacterium species are a key link between the gut microbiome and the systemic immune system. Differentially abundant associations between the bacterial species Eubacterium ventriosum and **(A)** immune cell populations/sub-types, and **(B)** metabolic pathways. Differentially abundant associations between **(C)** quartile 4 (Q4) colonic pH and Eubacterium rectale- and Eubacterium sp CAG 38- specific metabolic pathways. Only significant associations (q<0.05) are depicted. In panel A, coefficient of enrichment (β) quantifies the direction and strength of the association, with standard errors (SE) shown as horizontal error bars. In panel B, the size of the points corresponds to the significance of the association (−log10 (FDR)), and the point colour intensity reflects the scaled effect size (coefficient, β), with stronger colours indicating larger effect sizes. Immune cell types in bold overlap in both analyses. In panel C, association strength is represented by the weighted –log10(FDR). Figures were generated with the ggplot2 R package (v3.5.2). n=48-53. CCR7, C-C chemokine receptor type 7; CM, central memory; IFN-γ, interferon- γ; T regs, T regulatory cells; IL-, interleukin-; PD-1, programmed cell death protein 1; HLA-DR, human leukocyte

antigen-DR isotype; PMDSCs, polymorphonuclear myeloid-derived suppressor cells; TNF-α, tumour necrosis factor- α; NK, natural killer.

Figure 6. Eubacterium species connect microbiome, colonic pH and the systemic immune system. Alluvial diagram showing the connections between significant MetaCyc pathways, bacterial genus and associated species and biological variables, including quartile 4 (Q4) colonic pH and specific immune cell populations/sub-types. Link widths are weighted by the strength of association (−log10(FDR)). Out of all significant associations detected, these immune cell types, Q4, and metabolic pathways are linked through the Eubacterium genus. Only significant associations ($q<0.05$) are depicted. Figure was generated using the ggplot2 (v3.5.2) and ggalluvial (v0.12.5) R packages. n=48-53. CM, central memory; IL-, interleukin-; PD-1, programmed cell death protein 1; HLA-DR, human leukocyte antigen-DR isotype; TNF-α, tumour necrosis factor- α; NK, natural killer; T regs, T regulatory cells.

Figures

Figure 1

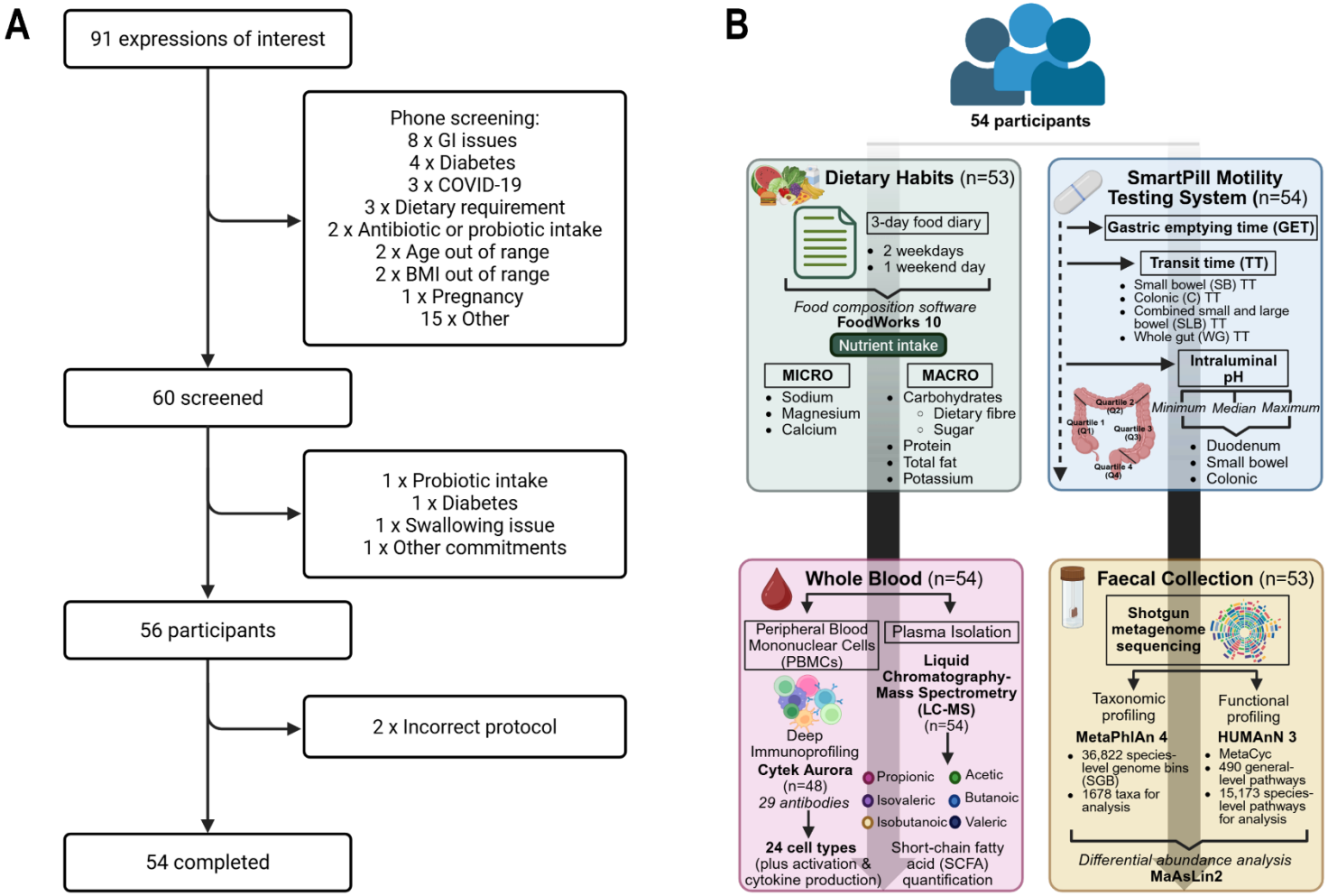

Figure 2

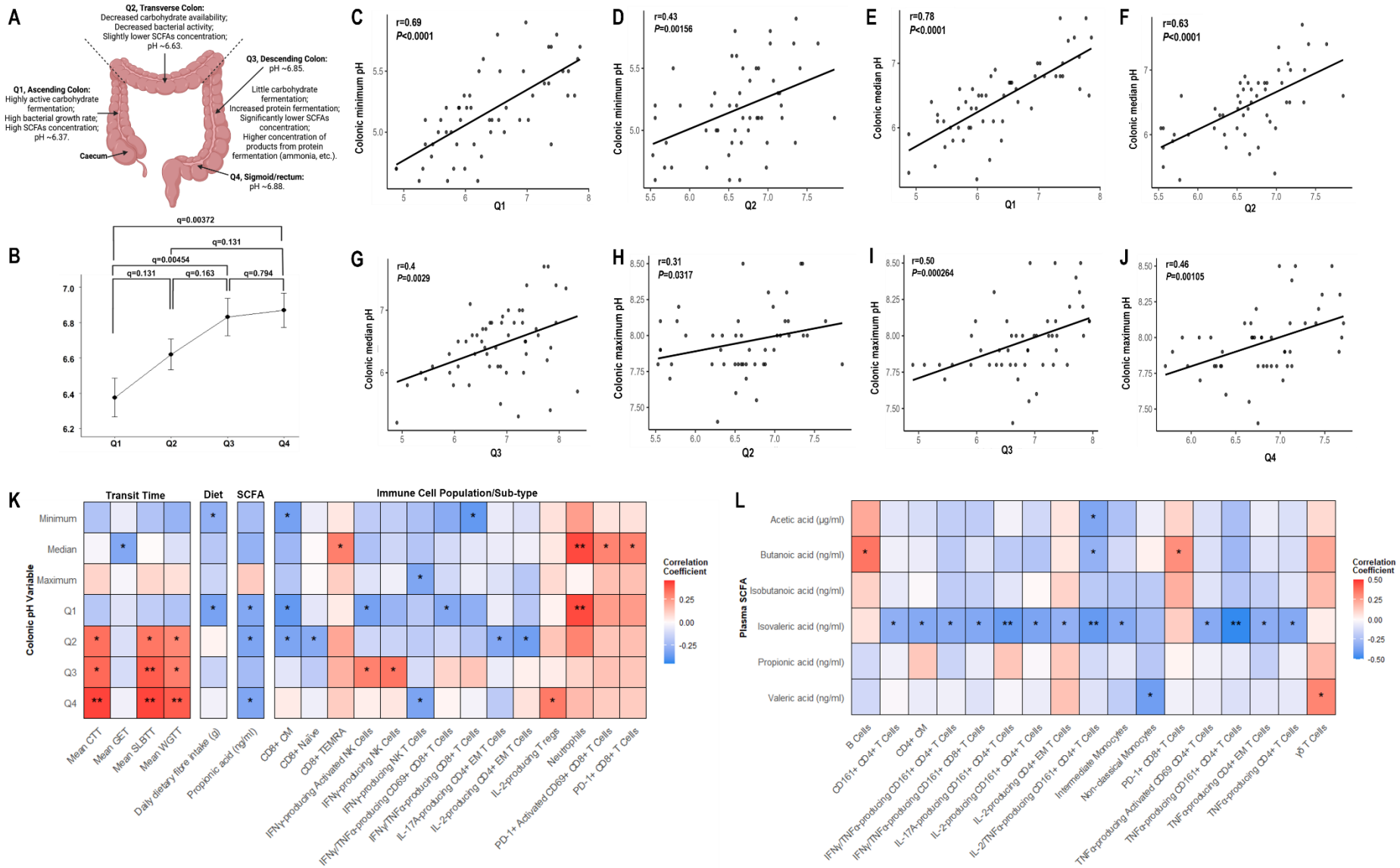
A
Q2, Transverse Colon:
Decreased carbohydrate availability;
Decreased bacterial activity;
Slightly lower SCFAs concentration;
pH ~6.63.
Q3, Descending Colon:
pH ~6.85.
Little carbohydrate fermentation;
Increased protein fermentation;
Significantly lower SCFAs concentration;
Higher concentration of products from protein fermentation (ammonia, etc.).
Q1, Ascending Colon:
Highly active carbohydrate fermentation;
High bacterial growth rate;
High SCFAs concentration;
pH ~6.37.
Caecum
Q4, Sigmoid/rectum:
pH ~6.88.
B
q=0.00372
q=0.131
q=0.00454
q=0.131
q=0.163
q=0.794
Q1
Q2
Q3
Q4
C
r=0.69
P<0.0001
Colonic minimum pH
Q1
D
r=0.43
P=0.00156
Colonic minimum pH
Q2
E
r=0.78
P<0.0001
Colonic median pH
Q1
F
r=0.63
P<0.0001
Colonic median pH
Q2
G
r=0.4
P=0.0029
Colonic median pH
Q3
H
r=0.31
P=0.0317
Colonic maximum pH
Q2
I
r=0.50
P=0.000264
Colonic maximum pH
Q3
J
r=0.46
P=0.00105
Colonic maximum pH
Q4
K
Transit Time
Diet
SCFA
Immune Cell Population/Sub-type
Colonic pH Variable
Minimum
Median
Maximum
Q1
Q2
Q3
Q4
Mean CTT
Mean GET
Mean SLBTT
Mean WGTT
Daily dietary fibre intake (g)
Propionic acid (ng/ml)
CD8+ CM
CD8+ Naïve
CD8+ TEMRA
IFNγ-producing Activated NK Cells
IFNγ-producing NK Cells
IFNγ-producing NK T Cells
IFNγ/TNFα-producing CD69+ CD8+ T Cells
IFNγ/TNFα-producing CD8+ T Cells
IL-17A-producing CD4+ EM T Cells
IL-2-producing CD4+ EM T Cells
IL-2-producing T regs
Neutrophils
PD-1+ Activated CD69+ CD8+ T Cells
PD-1+ CD8+ T Cells
Correlation Coefficient
0.25
0.00
-0.25
L
Plasma SCFA
Acetic acid (μg/ml)
Butanoic acid (ng/ml)
Isobutanoic acid (ng/ml)
Isovaleric acid (ng/ml)
Propionic acid (ng/ml)
Valeric acid (ng/ml)
B Cells
CD161+ CD4+ T Cells
CD4+ CM
IFNγ/TNFα-producing CD161+ CD4+ T Cells
IFNγ/TNFα-producing CD161+ CD8+ T Cells
IL-17A-producing CD161+ CD4+ T Cells
IL-2-producing CD161+ CD4+ T Cells
IL-2/TNFα-producing CD161+ CD4+ T Cells
Intermediate Monocytes
Non-classical Monocytes
PD-1+ CD8+ T Cells
TNFα-producing Activated CD69 CD4+ T Cells
TNFα-producing CD161+ CD4+ T Cells
TNFα-producing CD4+ EM T Cells
TNFα-producing CD4+ T Cells
γδ T Cells
Correlation Coefficient
0.50
0.25
0.00
-0.25
-0.50

Figure 3

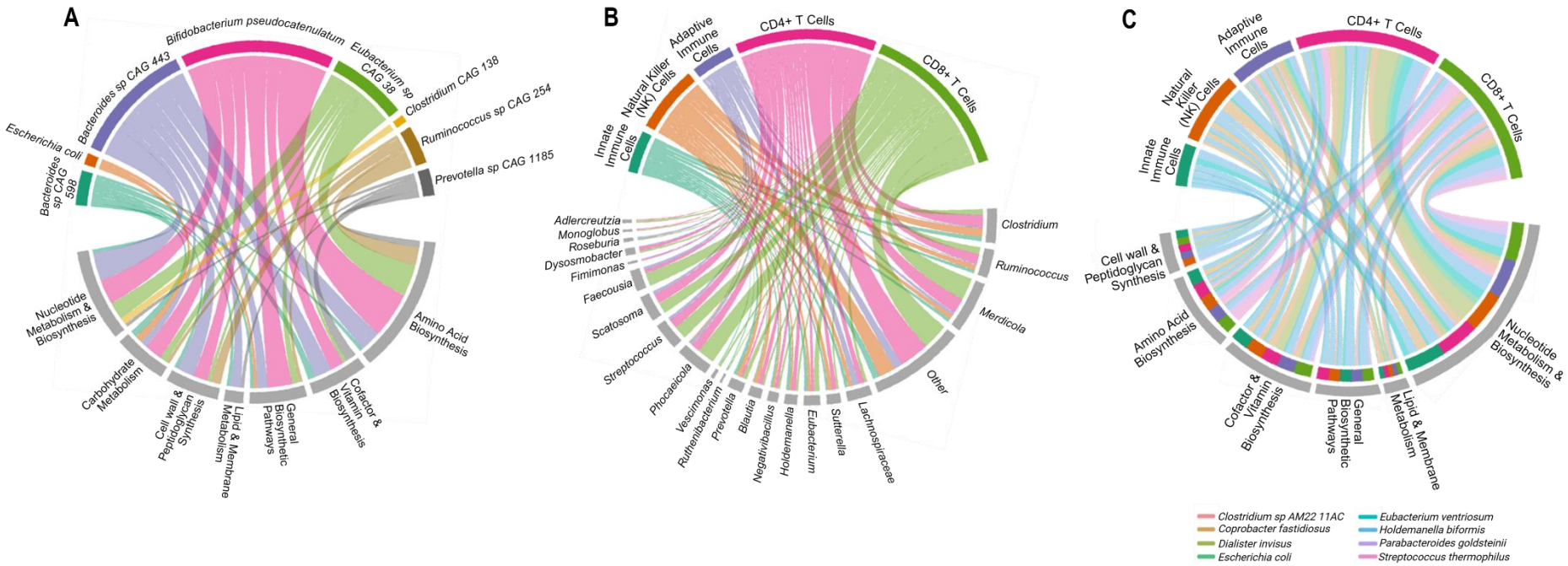
A
Bifidobacterium pseudocatenulatum
Eubacterium sp CAG 38
Clostridium CAG 138
Ruminococcus sp CAG 254
Prevotella sp CAG 1185
Bacteroides sp CAG 443
Escherichia coli
Bacteroides sp CAG 598
Nucleotide Metabolism & Biosynthesis
Carbohydrate Metabolism
Cell wall & Peptidoglycan Synthesis
Lipid & Membrane Metabolism
General Biosynthetic Pathways
Cofactor & Vitamin Biosynthesis
Amino Acid Biosynthesis
B
Adaptive Immune Cells
CD4+ T Cells
CD8+ T Cells
Natural Killer (NK) Cells
Innate Immune Cells
Adlercreutzia
Monoglobus
Roseburia
Dysosmobacter
Fimimonas
Faecousia
Scatosoma
Streptococcus
Phocaeicola
Vescimonas
Ruthenibacterium
Prevotella
Blautia
Negativibacillus
Holdemanella
Eubacterium
Sutterella
Lachnospiraceae
Other
Merdicola
Ruminococcus
Clostridium
C
Adaptive Immune Cells
CD4+ T Cells
CD8+ T Cells
Natural Killer (NK) Cells
Innate Immune Cells
Cell wall & Peptidoglycan Synthesis
Amino Acid Biosynthesis
Nucleotide Metabolism & Biosynthesis
Cofactor & Vitamin Biosynthesis
General Biosynthetic Pathways
Lipid & Membrane Metabolism
Clostridium sp AM22 11AC
Coprobacter fastidiosus
Dialister invisus
Escherichia coli
Eubacterium ventriosum
Holdemanella biformis
Parabacteroides goldsteinii
Streptococcus thermophilus

Figure 4

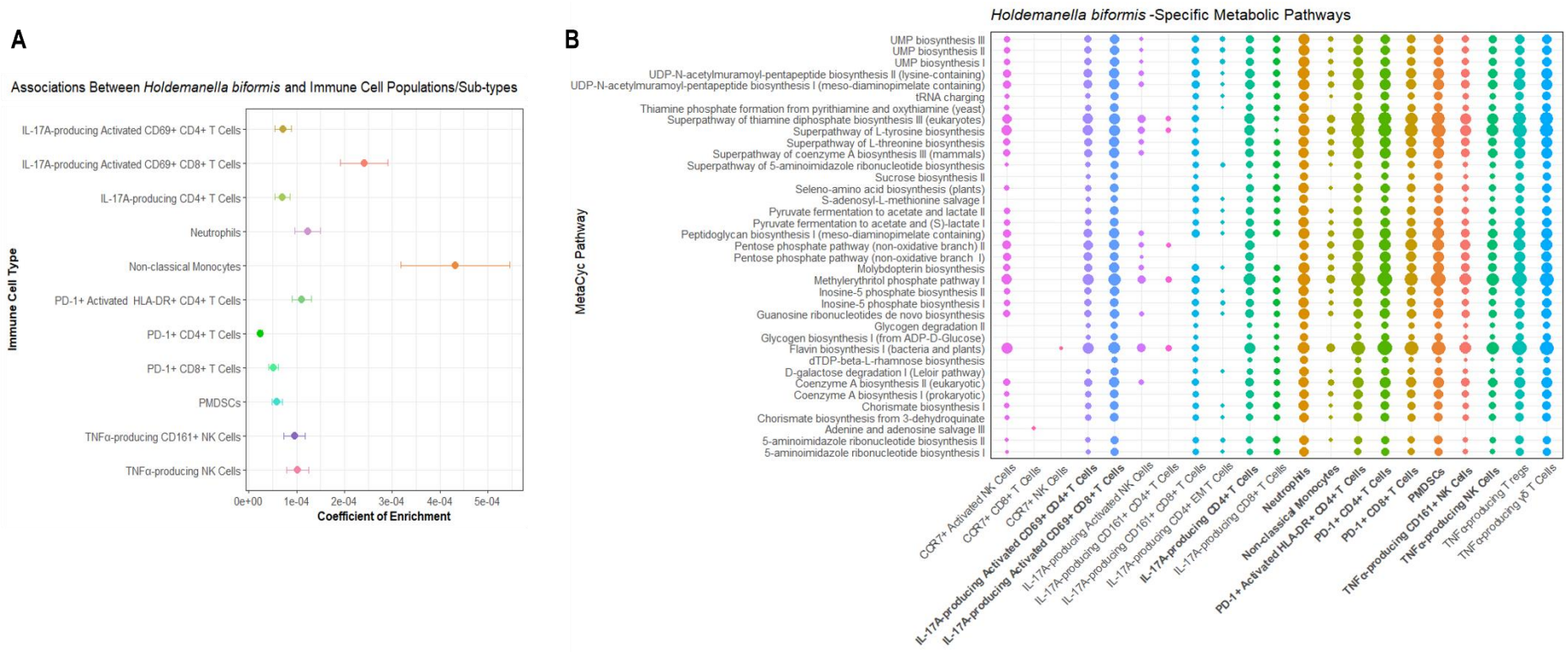
A
Associations Between Holdemanella biformis and Immune Cell Populations/Sub-types
Immune Cell Type
IL-17A-producing Activated CD69+ CD4+ T Cells
IL-17A-producing Activated CD69+ CD8+ T Cells
IL-17A-producing CD4+ T Cells
Neutrophils
Non-classical Monocytes
PD-1+ Activated HLA-DR+ CD4+ T Cells
PD-1+ CD4+ T Cells
PD-1+ CD8+ T Cells
PMDSCs
TNFα-producing CD161+ NK Cells
TNFα-producing NK Cells
0e+00
1e-04
2e-04
3e-04
4e-04
5e-04
Coefficient of Enrichment
B
Holdemanella biformis -Specific Metabolic Pathways
MetaCyc Pathway
UMP biosynthesis III
UMP biosynthesis II
UMP biosynthesis I
UDP-N-acetylmuramoyl-pentapeptide biosynthesis II (lysine-containing)
UDP-N-acetylmuramoyl-pentapeptide biosynthesis I (meso-diaminopimelate containing)
tRNA charging
Thiamine phosphate formation from pyrithiamine and oxythiamine (yeast)
Superpathway of thiamine diphosphate biosynthesis III (eukaryotes)
Superpathway of L-tyrosine biosynthesis
Superpathway of L-threonine biosynthesis
Superpathway of coenzyme A biosynthesis III (mammals)
Superpathway of 5-aminoimidazole ribonucleotide biosynthesis
Sucrose biosynthesis II
Seleno-amino acid biosynthesis (plants)
S-adenosyl-L-methionine salvage I
Pyruvate fermentation to acetate and lactate II
Pyruvate fermentation to acetate and (S)-lactate I
Peptidoglycan biosynthesis I (meso-diaminopimelate containing)
Pentose phosphate pathway (non-oxidative branch) II
Pentose phosphate pathway (non-oxidative branch I)
Molybdopterin biosynthesis
Methylerythritol phosphate pathway I
Inosine-5 phosphate biosynthesis II
Inosine-5 phosphate biosynthesis I
Guanosine ribonucleotides de novo biosynthesis
Glycogen degradation II
Glycogen biosynthesis I (from ADP-D-Glucose)
Flavin biosynthesis I (bacteria and plants)
dTDP-beta-L-rhamnose biosynthesis
D-galactose degradation I (Leloir pathway)
Coenzyme A biosynthesis II (eukaryotic)
Coenzyme A biosynthesis I (prokaryotic)
Chorismate biosynthesis I
Chorismate biosynthesis from 3-dehydroquinate
Adenine and adenosine salvage III
5-aminoimidazole ribonucleotide biosynthesis II
5-aminoimidazole ribonucleotide biosynthesis I
CCR7+ Activated NK Cells
CCR7+ CD8+ T Cells
CCR7+ NK Cells
IL-17A-producing Activated CD69+ CD4+ T Cells
IL-17A-producing Activated CD69+ CD8+ T Cells
IL-17A-producing Activated NK Cells
IL-17A-producing CD161+ CD4+ T Cells
IL-17A-producing CD161+ CD8+ T Cells
IL-17A-producing CD4+ EM T Cells
IL-17A-producing CD4+ T Cells
IL-17A-producing CD8+ T Cells
Neutrophils
Non-classical Monocytes
PD-1+ Activated HLA-DR+ CD4+ T Cells
PD-1+ CD4+ T Cells
PD-1+ CD8+ T Cells
PMDSCs
TNFα-producing CD161+ NK Cells
TNFα-producing NK Cells
TNFα-producing T regs
TNFα-producing γδ T Cells

Figure 5

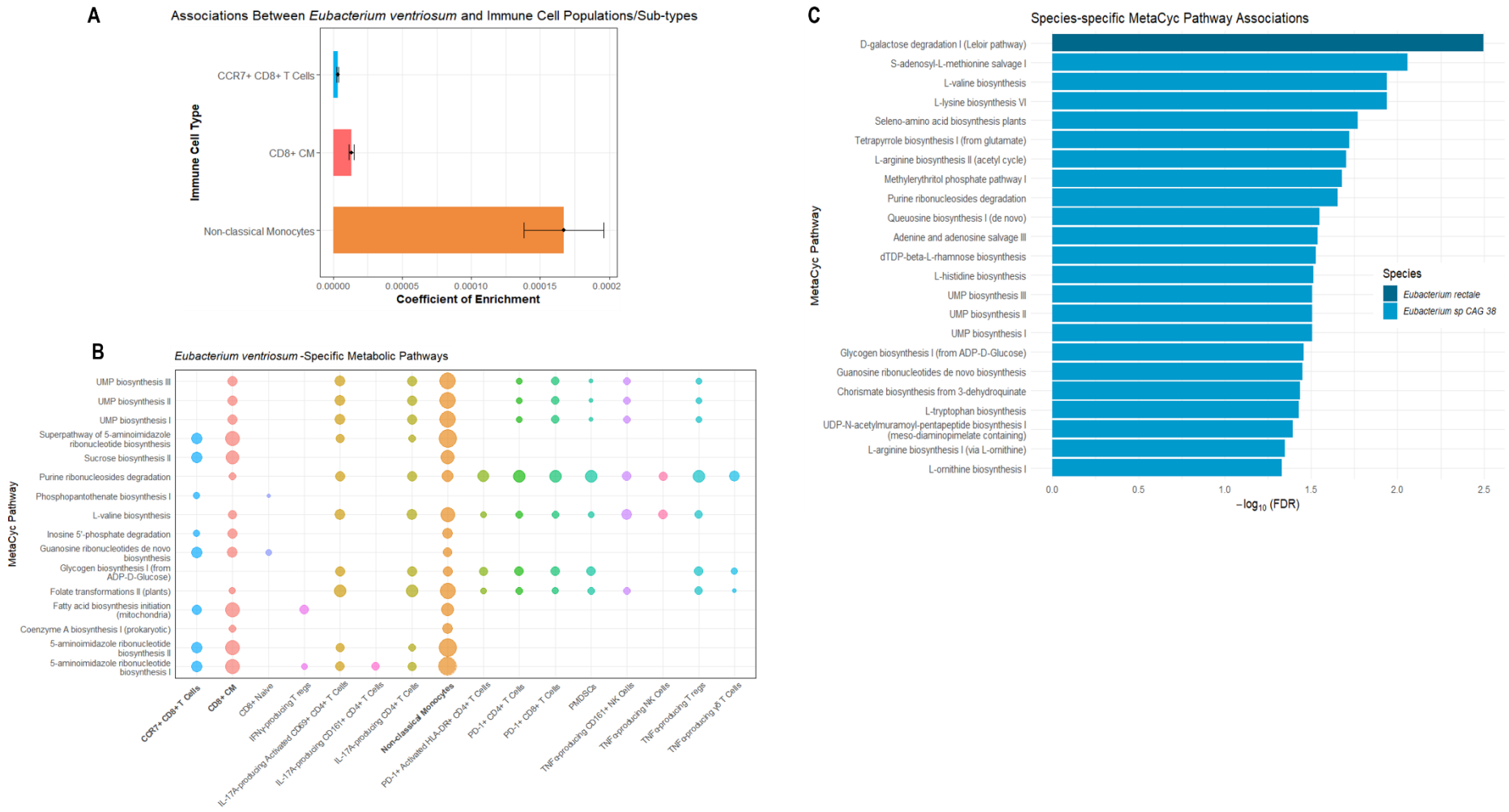
A
Associations Between Eubacterium ventriosum and Immune Cell Populations/Sub-types
Immune Cell Type
CCR7+ CD8+ T Cells
CD8+ CM
Non-classical Monocytes
0.00000
0.00005
0.00010
0.00015
0.0002
Coefficient of Enrichment
B
Eubacterium ventriosum -Specific Metabolic Pathways
MetaCyc Pathway
UMP biosynthesis III
UMP biosynthesis II
UMP biosynthesis I
Superpathway of 5-aminoimidazole ribonucleotide biosynthesis
Sucrose biosynthesis II
Purine ribonucleosides degradation
Phosphopantothenate biosynthesis I
L-valine biosynthesis
Inosine 5'-phosphate degradation
Guanosine ribonucleotides de novo biosynthesis
Glycogen biosynthesis I (from ADP-D-Glucose)
Folate transformations II (plants)
Fatty acid biosynthesis initiation (mitochondria)
Coenzyme A biosynthesis I (prokaryotic)
5-aminoimidazole ribonucleotide biosynthesis II
5-aminoimidazole ribonucleotide biosynthesis I
CCR7+ CD8+ T Cells
CD8+ CM
CD8+ Naive
IFNγ-producing T regs
IL-17A-producing Activated CD69+ CD4+ T Cells
IL-17A-producing CD161+ CD4+ T Cells
IL-17A-producing CD4+ T Cells
Nonclassical Monocytes
PD-1+ Activated HLA-DR+ CD4+ T Cells
PD-1+ CD4+ T Cells
PD-1+ CD8+ T Cells
PMDSCs
TNFα-producing CD161+ NK Cells
TNFα-producing NK Cells
TNFα-producing T regs
TNFα-producing γδ T Cells
C
Species-specific MetaCyc Pathway Associations
MetaCyc Pathway
D-galactose degradation I (Leloir pathway)
S-adenosyl-L-methionine salvage I
L-valine biosynthesis
L-lysine biosynthesis VI
Seleno-amino acid biosynthesis plants
Tetrapyrrole biosynthesis I (from glutamate)
L-arginine biosynthesis II (acetyl cycle)
Methylerythritol phosphate pathway I
Purine ribonucleosides degradation
Queuosine biosynthesis I (de novo)
Adenine and adenosine salvage III
dTDP-beta-L-rhamnose biosynthesis
L-histidine biosynthesis
UMP biosynthesis III
UMP biosynthesis II
UMP biosynthesis I
Glycogen biosynthesis I (from ADP-D-Glucose)
Guanosine ribonucleotides de novo biosynthesis
Chorismate biosynthesis from 3-dehydroquinate
L-tryptophan biosynthesis
UDP-N-acetylmuramoyl-pentapeptide biosynthesis I (meso-diaminopimelate containing)
L-arginine biosynthesis I (via L-ornithine)
L-ornithine biosynthesis I
0.0
0.5
1.0
1.5
2.0
2.5
−log10 (FDR)
Species
Eubacterium rectale
Eubacterium sp CAG 38

Figure 6

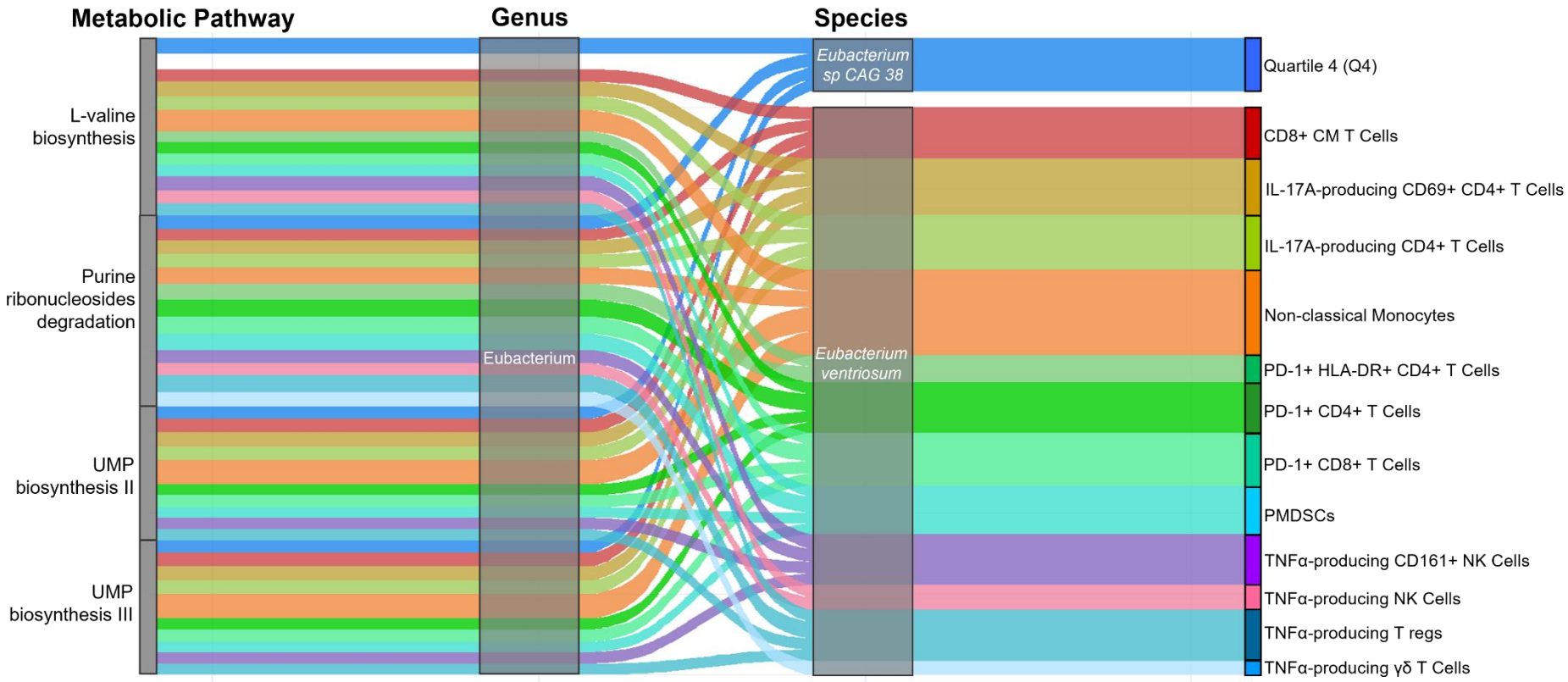
Metabolic Pathway
Genus
Species
L-valine biosynthesis
Purine ribonucleosides degradation
UMP biosynthesis II
UMP biosynthesis III
Eubacterium
Eubacterium sp CAG 38
Eubacterium ventriosum
Quartile 4 (Q4)
CD8+ CM T Cells
IL-17A-producing CD69+ CD4+ T Cells
IL-17A-producing CD4+ T Cells
Non-classical Monocytes
PD-1+ HLA-DR+ CD4+ T Cells
PD-1+ CD4+ T Cells
PD-1+ CD8+ T Cells
PMDSCs
TNFα-producing CD161+ NK Cells
TNFα-producing NK Cells
TNFα-producing T regs
TNFα-producing γδ T Cells